A closed-form solution for column-supported embankments with geosynthetic reinforcement

Lin-Shuang ZHAO[1], Wan-Huan ZHOU[*, 2], Xueyu GENG[3], Ka-Veng YUEN [4] and Behzad FATAHI[5]

Initials and Surname of all Authors:
L. S., ZHAO; W. H., ZHOU; K. V., YUEN; B., FATAHI
Current email address of ALL authors:
z.l.s0319@gmail.com, hannahzhou@umac.mo, xueyu.geng@warwick.ac.uk, kvyuen@umac.mo, Behzad.Fatahi@uts.edu.au

1 PhD Candidate, Department of Civil and Environmental Engineering, Faculty of Science and Technology, University of Macau, Macau, China. Email: z.l.s0319@gmail.com

2 Associate Professor (PhD, M. ASCE), Department of Civil and Environmental Engineering, Faculty of Science and Technology, University of Macau, Macau, China and UMacau Research Institute, Zhuhai, Guangdong, China. Email: hannahzhou@umac.mo

3. Assistant Professor in Geotechnical Engineering (BEng, MSc, PhD, FGS), School of Engineering (F332), The University of Warwick, Coventry, CV4 7AL, UK. Email: xueyu.geng@warwick.ac.uk

4 Professor, Department of Civil and Environmental Engineering, Faculty of Science and Technology, University of Macau, Macau, China. Email: kvyuen@umac.mo

5 Associate Professor, School of Civil and Environmental Engineering, University of Technology Sydney, Sydney, Australia. Email: Behzad.Fatahi@uts.edu.au

*Corresponding Author: E11-3014, Department of Civil and Environmental Engineering
Faculty of Science and Technology
University of Macau
Avenida da Universidade, Taipa, Macau, China
Tel: (+853) 8822 4469; Fax: (+853) 8822 2426
Email: hannahzhou@umac.mo

A closed-form solution for column-supported embankments with geosynthetic reinforcement

Lin-Shuang Zhao, Wan-Huan Zhou, Xueyu Geng, Ka-Veng Yuen and Behzad Fatahi

Abstract

Soil arching effect results from the non-uniform stiffness in a geosynthetic-reinforced and column-supported embankment system. However, most theoretical models ignore the impact of modulus difference on the calculation of load transfer. In this study, a generalized mathematical model is presented to investigate the soil arching effect, with consideration given to the modulus ratio between columns and the surrounding soil. For simplification, a cylindrical unit cell is drawn to study the deformation compatibility among embankment fills, geosynthetics, columns, and subsoils. A deformed shape function is introduced to describe the relationship between the column and the adjacent soil. The measured data gained from a full-scale test are applied to demonstrate the application of this model. In the parametric study, certain influencing factors, such as column spacing, column length, embankment height, modulus ratio, and tensile strength of geosynthetic reinforcement, are analyzed to investigate the performance of the embankment system. This demonstrates that the inclusion of a geosynthetic reinforcement or enlargement of the modulus ratio can increase the load transfer efficiency. When enhancing the embankment height or applying an additional loading, the height of the load transfer platform tends to be reduced. However, a relatively long column has little impact on the load transfer platform.

Keywords: Geosynthetics; column-supported embankment; soil arching; modulus ratio; stress ratio; axisymmetric modelling.

1. Introduction

A column supported embankment (Ali et al., 2012; Okyay et al., 2014; Basack et al., 2015; Bian et al., 2016; Liu and Rowe, 2016; Liyanapathirana and Ekanayake, 2016; Briançon and Simon, 2017; Das and Deb, 2017a; Jelušič and Žlender, 2018) is commonly used when freeways or railways pass through soft soil areas, or to support storage tanks and bridge abutments (Naggar et al., 2015). This technique can reduce settlement (Tan et al., 2008; Yapage and Liyanapathirana, 2014; Yapage et al., 2015; Chen et al., 2016a; Das and Deb, 2017b; King et al., 2017) and accelerate the construction process (Briançon and Simon, 2012; Fagundes et al., 2017; Nguyen et al., 2017). However, the most significant drawback of this approach is the possible localized differential settlement at the surface of the embankment, caused by the difference between the modulus of the columns and that of the subsoil (Taha et al., 2014; Tai et al., 2018). The latter tends to experience greater displacement than that of the columns; the part of the embankment fill (*part B*) above the subsoil moves downward to supplement this void. Meanwhile, this downward movement is resisted by the embankment fill (*part A*) overlying the column. Load transfer occurs between *part A* and *part B* because of the shear resistance, resulting in an increase in stress in *part A* above the column and a decrease in stress in *part B* above the subsoil. This load transfer is also referred to as the soil arching effect (Iglesia et al., 2014; Girout et al., 2016; Huckert et al., 2016; Rui et al., 2016; Smith and Tatari, 2016; Villard et al., 2016; Ghazavi et al., 2018; Girout et al., 2018; King et al., 2018; Pham et al., 2018). Usually, a load transfer platform is constructed above the top of the columns to eliminate this differential settlement, and one or several layers of geosynthetic reinforcements (Shukla and Chandra, 1994; Hinchberger and Rowe, 2003; Rowe and Li, 2005; Ariyarathne et al., 2013; Abu-Farsakh et al., 2016; Zhao et al., 2016; Da Silva et al., 2017; Feng et al., 2017a; Ghosh et al., 2017a, 2017b) are sandwiched therein to strengthen the load transfer platform. Some researchers have applied fiber or tire mixtures to improve the strength of this platform (Bordoloi et al., 2015; Zhang et al., 2015a, 2015b; Disfani et al., 2017; Bordoloi et al., 2018; Indraratna et al., 2018). Because the shear resistance in the embankment fill is significant in the soil arching effect, the grain size distribution should be well designed to prevent erosion caused by water flow (Premkumar et al., 2016). Some scholar (Bhasi and Rajagopal, 2015) have also considered the difference between the end-bearing and floating columns and studied their influence on the soil arching effect. The end-bearing columns may be of various types, such as concrete piles, semi-deep soil-mixing columns, stone columns, and so on. For the rigid columns, such as concrete piles, only minor compression occurs at the pile top under the load from the embankment fill and vehicles. Han and Gabr (2002) applied the finite element method to investigate a pile-supported embankment with geosynthetic reinforcement and introduced the concept of stress ratio to evaluate the stress concentration. Liu et al. (2007), meanwhile, carried out a full-scale test on the geosynthetic-reinforced and pile-supported embankment, monitoring the stresses and settlements. Chen et al. (2008b) then proposed a theoretical model for the rigid piled embankment. Finally, Van Eekelen et al. (2013) used the concentric arches theory to study the soil arching effect. To obtain a conservative design, the support of subsoil is commonly ignored in rigid piled embankments. However, for a semi-rigid column-supported embankment, the semi-rigid column has a relatively large compressive deformation, which results in a smaller deformation difference between the column and the subsoil. This releases the stress concentration on the columns, and some of the load coming from the embankment fill is supported by the surrounding soil. The direct use of the existing analytical methods for rigid piles, to evaluate the semi-rigid column-supported embankments in real practice, commonly produces a large column diameter with a relatively small column spacing, which is not economically practicable. This issue has attracted the attention of many engineers and researchers, and a handful of studies have been conducted to evaluate the geosynthetic-reinforced and semi-rigid column-supported embankments. These vary from laboratory tests (Chen et al., 2008a; Van Eekelen et al., 2012a, 2012b; Xu et al., 2016; Debnath and Dey, 2017; Esmaeili et al., 2017; Mehdizadeh et al., 2018) to full-scale experiments (Chen et al., 2010; Liu et al., 2012; Hong et al., 2014; Weng et al., 2014; Liu et al., 2015; Rowe and Liu, 2015; Van Eekelen et al., 2015; Cao et al., 2016; Van Eekelen et al., 2017; Michalowski et al., 2018; Tano et al., 2018; Wang et al., 2018a, 2018c) and from analytical models (Balaam and Booker, 1981; Deb, 2010; Karim et al., 2011; Van Eekelen et al., 2011, 2013; Zhou et al., 2012; Yang et al., 2013; Zhuang et al., 2014; Jamsawang et al., 2016; Van Eekelen, 2016; Feng et al., 2017b; Zhao et al., 2017) to numerical simulations (Huang and Han, 2009; Jiang et al., 2014; Kamash and Han, 2014; Lai et al., 2014; Yoo, 2015; Zhuang and Wang, 2015; Liu et al., 2017; Zhou et al., 2017; Wijerathna and Liyanapathirana, 2018).

Some researchers (Li and Rowe, 2008; Ariyarathne and Liyanapathirana, 2015; Feng et al., 2015; Rowe and Liu, 2015; Yu et al., 2016; Zhang et al., 2016) have found that the geosynthetic reinforcement is significant in load transfer platforms. The geosynthetics can enhance load transfer efficiency and diminish differential settlements. Using Hewlett and Randolph’s (1988) semi-spherical crown model, Low et al. (1994) introduced geosynthetic reinforcement and drew up charts to evaluate the load transfer when adopting a geosynthetic layer. In BS8006 (2010), the geosynthetic reinforcement is designed in a conservative manner, assuming that no support comes from the underlying soil. Abusharar et al. (2009) carried out a theoretical analysis under two-dimensional plane-strain assumption. The shape of geosynthetics after deformation is presumed to be a circular arc, and the shear resistance between soil and geosynthetics is considered. Some scholars (Halvordson et al., 2010; Jones et al., 2010; Plaut and Filz, 2010) have adopted the three-dimensional thin-plate model, cable-net model, and axisymmetric model to simulate the behavior of geosynthetic reinforcement. Chen et al. (2016b) carried out a full-scale test to measure the tensile force of the geogrid in different scenarios. Van Eekelen et al. (2012a, 2012b), meanwhile, performed a series of three-dimensional laboratory experiments, concluding that the load distribution on the geosynthetic reinforcement is in an inverse triangle shape and making an attempt to improve the existing design method in EBGEO (2010). Deb and Mohapatra (2013), for their part, examined the variation in the geosynthetic reinforcement, considering the support of the underlying subsoil using a multiplying factor. Later, Zhuang and Wang (2016) presented a finite element analysis of the piled embankment with reinforcement, finding that the introduced geogrid reinforcement can significantly relieve the load supported by the foundation soil and reduces the differential settlement. However, the authors of these recent studies tend to ignore the deformed shape of geosynthetic reinforcement or assume it to be an arc or catenary without considering the support from subsoils. However, in real practice, especially for the semi-rigid columns, the deformation of the geosynthetic layer can be affected by the behavior of the overlying embankment as well as the underlying foundation soil. Great difficulties are involved in capturing the actual shape of the geosynthetic reinforcement. Few researchers have paid attention to the deformation shape of the geosynthetics in an embankment system, especially including the stress and deformation compatibility.

In this study, the non-uniform stiffness of the column-embedded subsoil and the deformation of the geosynthetic reinforcement are considered, and a closed-form solution is proposed for a geosynthetic-reinforced and column-supported embankment. The formulation process of the theoretical model is presented, and the feasibility of the proposed solution is validated using measured data. A parametric study is performed to evaluate certain significant factors, such as the modulus ratio, tensile strength of geosynthetics, column spacing, column length, and embankment height. The load transfer efficiency is discussed and the height of the equal settlement plane evaluated.

2. Mathematical modeling

In this study, a cylindrical unit cell (Smith and Filz, 2007) was built to describe the behavior of a geosynthetic-reinforced and column-supported embankment. It was applied to the columns close to the middle section of the embankment, but not to those at the embankment toe. As shown in Fig. 1, the area equivalence technique was adopted to calculate the outer diameter of the cylindrical unit cell, given the column spacing. Keeping this outer diameter and extending the cylinder into the embankment fill, it formed the whole unit cell (Fig. 2(a)), which contained a column, the influenced zone of subsoil, and a circular shape of geosynthetics, as well as the embankment fill. The observer should note that one-dimensional compression was assumed for the aforementioned components in the unit cell. The included embankment fill was divided into two parts by extending the cylinder of the column into the embankment fill virtually. This produced an inner cylinder (*part A*) together with an outer hollow cylinder (*part B*), as presented in Fig. 2(a). The shear at the interface between these two parts of the embankment fill was adopted to model the load transfer because of the differential settlement. Although such an assumption may not reveal the exact interactions within the embankment fill, it can capture the main features of the load transfer. In Chen et al.'s (2008b) theoretical model, they applied this idealization in a piled embankment.

2.1 Embankment fill in the unit cell

In the unit cell, because of the relatively larger displacement in the surrounding soil than that in the column, differential settlement develops between the inner cylinder (*part A*) and the outer hollow cylinder (*part B*). With the raising of the embankment height, this differential settlement diminishes, finally reaching a plane where no such settlement exists. This was named the equal settlement plane by Terzaghi (1943). The reader should note that the deformation difference below the equal settlement plane triggers the shear resistance between *part A* and *part B* and that the shear stress is kept at the ultimate state up to the equal settlement plane (Fig. 2(a-1)). Given the vertical stress, σ, under K_0 assumption, the shear stress at the ultimate state is:

$$f = \sigma K_0 \tan\varphi \tag{1}$$

where $K_0 = 1 - \sin\varphi$. φ means the internal friction angle associated with the embankment.

As shown in Fig. 2(b), the original point is located at the center of the column top. The positive direction of the z axis is downward. For an arbitrary small element in the inner cylinder, as shown in Fig. 2(d-1), this should satisfy the vertical force equilibrium. Assuming that the thickness and cross section area of the element are dz, and A_i, respectively, the force increment at the cross section of this element can be written as:

$$A_i d\sigma_i(z) = (\gamma A_i + \pi d_c f)dz \tag{2}$$

where γ denotes the unit weight of the embankment and $\sigma_i(z)$ describes the vertical stress at the depth of z.

According to the definition of the equal settlement plane, no load transfer happens there, and it should be at a geostatic pressure state. Hence, the vertical stress at the plane is formulated as per the following equation and is the upper bound of Eq. (2):

$$\sigma\big|_{z=-h_e} = \gamma(h - h_e) + q_u \tag{3}$$

where h_e is the distance between the column top and the equal settlement plane, h is the total height of the embankment, and q_u is the additional loading.

To solve Eq. (2), while integrating it on both sides with the range of [-h_e, 0] (Fig. 2(a-1)), the vertical stress in the inner cylinder can be gained as:

$$\sigma_i(z) = \frac{\gamma d_c}{4K_0 \tan\varphi}\left\{\left[1+\frac{4K_0 \tan\varphi}{d_c\gamma}\left(\gamma\left(h-h_e\right)+q_u\right)\right]\exp\left(4K_0 \tan\varphi\frac{z+h_e}{d_c}\right)-1\right\} \quad (4)$$

In Eq. (4), to calculate the distribution of σ_i, the unknown parameter h_e should be determined, which is relevant to the deformation calculation of the foundation soil embedded within columns.

Next, the expression for the vertical stress $\sigma_o(z)$, in the outer hollow cylinder, will be calculated. Based on the assumption of the cylindrical unit cell, no friction exists at the outer boundary. At any cross-section of the inner cylinder (and outer hollow cylinder), the stresses are assumed to be in a uniform distribution. According to Fig. 2(a), $\sigma_i(z)$ and $\sigma_o(z)$ should balance with the self-weight of the embankment fill and the additional loading, which can be written as:

$$\sigma_i(z)A_i + \sigma_i(z)\left(\frac{\pi d_e^2}{4} - A_i\right) = \left[\gamma\left(h+z\right)+q_u\right]\frac{\pi d_e^2}{4} \quad (5)$$

Using the calculated $\sigma_i(z)$ and $\sigma_o(z)$ in Eq. (5), the differential settlement S_e (Fig. 2(a-1)), at the bottom of the embankment can be calculated as:

$$S_e = \int_{-h_e}^{0} \frac{\sigma_i(z)-\sigma_o(z)}{E_f}dz \quad (6)$$

where E_f refers to the compressive modulus of the embankment material. Associating Eqs. (4)–(5) with Eq. (6), the following formula can be obtained:

$$S_e = \frac{1}{E_f}\left(1+\frac{A_i}{A_o}\right)\left\{\frac{\gamma d_c^2}{16K_0^2 \tan^2\varphi}\exp\left(\frac{\gamma d_c h_e}{4K_0\tan\varphi}\right)\left[1+\frac{4K_0\tan\varphi}{d_c}\left(h-h_e\right)\right]\right.$$
$$\left.-\frac{\gamma d_c^2}{16K_0^2\tan^2\varphi}\left[1+\frac{4K_0\tan\varphi}{d_c}\left(h-h_e\right)\right]-\frac{\gamma d_c h_e}{4K_0\tan\varphi}-\gamma\left(hh_e-\frac{1}{2}h_e^2\right)-q_u h_e\right\} \tag{7}$$

At this point, the expression of the differential settlement has been obtained but the parameter, h_e, remains unknown. The differential settlement, S_e, should be accompanied by the deformation of the column-reinforced foundation to establish the volume continuity of the entire unit cell. In the following part, both the vertical deformations of the column and the foundation soil are presented.

2.2 Behavior of column embedded subsoil

Because of the load coming from the embankment fill, vertical displacements develop in the column and the surrounding subsoil. The friction at the column shaft leads to the development of a relatively small vertical displacement around the column and this displacement increases with the distance far away from the column shaft. Note that negative skin friction develops at the column shaft, increasing the stress and compression on the column and reducing the stress and compression in the surrounding soil. The deformation shape of the latter is hard to determine and is influenced by certain factors, such as soil structure interactions (Zhou and Yin, 2008; Yin and Zhou, 2009; Su et al., 2010; Zhou et al., 2011; Hokmabadi et al., 2014; Suleiman et al., 2016; Meguid et al., 2017; Yu and Bathurst, 2017; Zhu et al., 2017; Jing et al., 2018; Wang et al., 2018b) and constitutive models adopted for subsoil (Yin et al., 2009, 2010a, 2010b, 2011a, 2011b; Sexton et al., 2016; Yin et al., 2017). Alamgir et al. (1996) innovatively proposed a deformed shape function to investigate the performance of a column-reinforced foundation, which is applied here for this purpose.

Based on Alamgir et al.'s model (1996), the vertical deformation in the surrounding soft soil, $w(r, z)$ (Fig. 2(a-1)), at a depth of z and with a radius distance of r ($d_c/2 \le r \le d_e/2$), can be written as:

$$w(r,z)=w_c(z)+\alpha_c(z)\left[\frac{2r}{d_c}-\exp\left(\beta_c\frac{2r}{d_c}-\beta_c\right)\right] \quad (8)$$

where $w_c(z)$ stands for the vertical displacement in the column. β_c is related to the size of the unit cell and $\alpha_c(z)$ denotes the deformation factor, which will be calculated in a later section.

In the following derivation process, the column and foundation soil are assumed to be homogenous materials with constant modulus and Poisson's ratio (E_c and v_c for the column, E_s and v_s for the foundation soil). Because the shear strain is vital to an analysis of the deformation behavior of subsoil, it can be calculated by differentiating Eq. (8) regarding the variable, r:

$$\gamma(r,z)=\frac{\partial s(r,z)}{\partial r}=\frac{2\alpha_c(z)}{d_c}\left[1-\beta_c e^{\beta_c\left(2r/d_c-1\right)}\right] \quad (9)$$

Based on $G_s = E_s/2(1+v_s)$, by multiplying Eq. (9) by the shear modulus, G_s, the shear stress can be determined using the following expression:

$$\tau(r,z)=\frac{\partial s(r,z)}{\partial r}=\frac{E_s\alpha_c(z)}{d_c(1+v_s)}\left[1-\beta_c e^{\beta_c\left(2r/d_c-1\right)}\right] \quad (10)$$

Based on the assumptions made in the cylindrical unit cell, the outer boundary should be at the central line between two adjacent columns. The shear stress at this position is zero:

$$\tau\left(\frac{d_o}{2},z\right)=0 \quad (11)$$

Associating Eq. (11) with Eq. (10), the parameter, β_c, can be calculated as:

$$\beta_c e^{\beta_c(d_e/d_c-1)}-1=0 \quad (12)$$

To calculate the deformation parameter, α_c, the deformation relationship between the column and the adjacent subsoil should be established. The following equations illustrate the deformations of the column and the subsoil. To facilitate the calculation, the column in the unit cell is separated equally into N elements while the surrounding soil is meshed into $N\times M$ elements (Fig. 2(d)).

For the j^{th} element in the column (Fig. 2(d-2)), the following equation is formulated:

$$\frac{d\sigma_c(z)}{dz}=\frac{4}{d_c}\tau\left(\frac{d_c}{2},z\right) \tag{13}$$

Associating Eq. (10) with Eq. (13) gives us the following formula:

$$\frac{d\sigma_c(z)}{dz}=\frac{4E_s(1-\beta_c)\alpha_c(z)}{d_c^2(1+v_s)} \tag{14}$$

According to the finite difference method, the relation between the vertical stress of the j^{th} element and that of the $(j+1)^{\text{th}}$ element can be calculated as:

$$\frac{\sigma_{c(j+1)}-\sigma_{cj}}{\Delta h}=\frac{4E_s\alpha_{cj}(1-\beta_c)}{d_c^2(1+v_s)} \tag{15}$$

where $\Delta h = l/N$.

The vertical deformation of the j^{th} element can be formulated as:

$$w_{cj}=\frac{\Delta h}{E_c}\sigma_{cj}+\left(\frac{2\Delta h}{d_c}\right)^2\frac{(1-\beta_c)E_s\alpha_{cj}}{2E_c(1+v_s)} \tag{16}$$

Based on the mesh of foundation soil, the geometry of one soil element is $\Delta h \times \Delta r$, where $\Delta r = (d_e - d_c)/M$ (Fig. 2(d-3)). Taking one element at the outer boundary, as shown in Fig. 2(d-4), the vertical force equilibrium of this element is:

$$\frac{d\sigma_{sM}(z)}{dz}=-\tau_M(z)\frac{2(n-\Delta R)}{d_c\omega} \tag{17}$$

where $n = d_e/d_c$, $\Delta R = 2\Delta r / d_c$, and $\omega = \Delta R(n-\Delta R/2)$. The subscript M refers to the element at the outer boundary.

Associating Eq. (10) with Eq. (17) results in:

$$\frac{d\sigma_{sM}(z)}{dz}=-\frac{2(n-\Delta R)\left[1-\beta_c e^{\beta_c(n-\Delta R-1)}\right]E_s\alpha_c}{d_c^2\omega(1+v_s)} \tag{18}$$

For the $(M, j)^{th}$ element (Fig. 2(d-4)) at the outer boundary of the unit cell, the relationship between the vertical stress on the upper side, $\sigma_{sM(j+1)}$, and that on the lower side, σ_{sMj}, of this element can be obtained using the finite difference method:

$$\frac{\sigma_{sM(j+1)}-\sigma_{sMj}}{\Delta h}=-\frac{2(n-\Delta R)\left[1-\beta_c e^{\beta_c(n-\Delta R-1)}\right]E_s\alpha_c(j)}{d_c^2\omega(1+v_s)} \tag{19}$$

Then, based on Eq. (19), the displacement change in the $(M, j)^{th}$ element is:

$$u_{sMj}=\frac{\Delta h}{E_s}\sigma_{sMj}-\frac{(\Delta h/d_c)^2(n-\Delta R)\left[1-\beta_c e^{\beta_c(n-\Delta R-1)}\right]\alpha_{cj}G_s}{\omega(1+v_s)} \tag{20}$$

Based on the assumptions made in the deformed shape function, no slip is allowed between the column shaft and the adjacent soil. According to the mesh, the $(M, j)^{th}$ element at the outer boundary of the unit cell and the j^{th} element in the column should be at the same depth; their deformations should be compatible in Eq. (8). The deformation relationship can be expressed as:

$$w_{sMj}=w_{cj}+\left[n-\frac{\Delta R}{2}-e^{\beta_c(n-\Delta R/2-1)}\right]\alpha_{cj} \tag{21}$$

Associating the deformation of the column element in Eq. (16) and that of the soil element in Eq. (20) with Eq. (21), the parameter, α_{cj}, can be calculated as:

$$\alpha_{cj} = \frac{\left[\sigma_{sNj} / E_s - \sigma_{cj} / E_c\right]\Delta h}{\left(B_1 + B_2 + B_3\right)} \tag{22}$$

where $B_1 = \left(\frac{2\Delta h}{d_c}\right)^2 \frac{\left(1-\beta_c\right)E_s}{2E_c\left(1+v_s\right)}$, $B_2 = \frac{\left(\Delta h\right)^2\left(n-\Delta R\right)\left[1-\beta_c e^{\beta_c\left(n-\Delta R-1\right)}\right]}{d_c^2 \Delta R\left(n-\Delta R/2\right)\left(1+v_s\right)}$,

$B_3 = n - \frac{\Delta R}{2} - e^{\beta_c\left(n-\Delta R/2-1\right)}$.

2.3 Deformation of geosynthetic reinforcement

In this study, a nonwoven geotextile is used, a kind of geosynthetics that is assumed to be isotropic. The function of geosynthetic reinforcement is to transfer some part of the load supported by the surrounding soil onto the adjacent columns. Because the geosynthetics cannot sustain any bending moment, they are assumed to deform compatibly with the column-reinforced foundation. As demonstrated in Fig. 2(b), the geosynthetics have the same deformed shape as the underlying foundation soil, which is simplified into a two-dimensional axisymmetric analysis. The vertical force equilibrium of the geosynthetic reinforcement is shown in Fig. 2(c-1). Its tensile force, T, can be expressed as:

$$\frac{\pi\left(d_e^2 - d_c^2\right)}{4}\sigma_u - \pi d_c T \sin\theta = \frac{\pi\left(d_e^2 - d_c^2\right)}{4}\sigma_b \tag{23}$$

where σ_u refers to the vertical stress acting on the top of the geosynthetics, while σ_b means the vertical stress on the foundation soil. θ is the rotation angle of the deformed geosynthetics (Fig. 2(c-1)) and can be determined as:

$$\theta = \frac{ds\left(r,0\right)}{dr} = \frac{\sum_{j=1}^{N} w_{s1j} - \sum_{j=1}^{N} w_{s2j}}{\Delta r} \tag{24}$$

where w_{s1j} and w_{s2j} are the displacement changes of the first and second soil element, respectively, adjacent to the column.

The tensile strain in the geosynthetics is not uniform: The maximum tensile strain in the geosynthetics is generated at the edge of the column (Liu et al., 2007; Van Eekelen et al., 2012a, 2012b; Chen et al., 2016b). As shown in Fig. 2(c), Δr is the length of one geosynthetics element at the edge of the column before deformation. Because of the vertical deformation of Δz, Δr is stretched into Δs. According to the geometry in Fig. 2(c), the tensile strain is:

$$\varepsilon = \frac{\Delta s - \Delta r}{\Delta r} = \frac{\sqrt{\Delta r^2 + \Delta z^2} - \Delta r}{\Delta r} = \sqrt{1 + \tan^2\theta} - 1 \tag{25}$$

By combining Eqs. (23)–(25), the tensile force, $T = \varepsilon_g \cdot K_g$, can be determined, where K_g is the tensile strength of geosynthetic reinforcement. In Chen et al.'s study (2016b), the tensile strength of geosynthetics is determined at the strain of $\varepsilon = 2\%$.

2.4 Deformation continuity

Using the calculated stress on the foundation soil and that on the column, the deformed volume of the foundation can be determined based on Eq. (8). This deformed volume is the precise volume coming from the differential deformation at the base of the embankment fill. Take note that, based on the assumption made in the embankment fill, the displacements at the bottom of the inner and outer hollow cylinders are uniform, which is not consistent with the deformed shape of the foundation settlement. However, a reasonable step is to adopt the volume equivalence to bridge the relationship between the embankment fill and the column-reinforced subsoil.

Based on the deformed shape function, the vertical displacement developed at the surface of the subsoil is:

$$S_t(i) = \sum_{j=1}^{j=N} w_{ij} \tag{26}$$

The volume equivalence between $S_t(i)$ and S_e can be formulated as:

$$\int_{\frac{d_c}{2}}^{\frac{d_e}{2}} S_t\left(i\right)\cdot 2\pi r dr = \int_{\frac{d_c}{2}}^{\frac{d_e}{2}} S_e 2\pi r dr \tag{27}$$

where i = 1, 2, 3, …, M means the i^{th} soil element. By combining Eqs. (7), (8), (22), (23), (26), and (27) together, the stresses within the embankment system and the tensile force in the geosynthetics can be obtained.

Han and Gabr (2002) presented the concept of the stress ratio to evaluate the load transfer efficiency. This is written in the following form:

$$\sigma_c / \sigma_s = \left.\frac{\sigma_i}{\sigma_o}\right|_{z=0} \tag{28}$$

where σ_c is the stress acting on the column top and σ_s denotes the stress sustained by the subsoil. This ratio is adopted in this study to illustrate the load transfer efficiency in different scenarios.

3. Comparison with a full-scale test and analytical models

3.1 Full-scale test

In this comparison, a full-scale test (Chen et al., 2016b; Zhou et al., 2016) carried out at Zhejiang University, was adopted to evaluate the proposed axisymmetric model. The pile caps were arranged in a 3×5 pattern. The surrounding soil was replaced with water bags, filled with water, to simulate the settlement of subsoil. A granular layer, sandwiched with a geosynthetic reinforcement, was placed overlying the pile caps. The embankment was then constructed step-by-step. Thereafter, the concrete base and rail plate, as a surcharge loading of 12.25 kPa, were paved on top of the constructed embankment. The parameters associated with the embankment system are illustrated in Table 1. Because it is an axisymmetric model in the proposed method, the diameters of the column and influencing surrounding soil were calculated based on the column width and spacing in the full-scale test (area equivalence).

The modulus ratio, E_c/E_s = 10, and the Poisson's ratio of subsoil, v_s = 0.35, were determined based on a trial-and-error process because these two parameters were not available in the full-scale test. The column length, l/d_c = 20, was selected so that the column length (i.e., the thickness of foundation soil) had no effect on the load transfer (Fig. 12). The observer should note that, in real practice, these parameters in the proposed model, such as the modulus ratio, E_c/E_s, the column length, and so on, can be determined from the field tests (Alamgir et al., 1996; Deb et al., 2013). To demonstrate the feasibility of the proposed model, the calculated results from the proposed model were compared with the measured data from a full-scale test (Chen et al., 2016b; Zhou et al., 2016). Two scenarios were considered, as shown in Table 2; one was at the end of the embankment construction, and the other came after paving the concrete base and rail plate. The reader should note that no gap exists between the embankment fill and the underlying water bags in these two scenarios. The comparison illustrates that the proposed solutions are close to the measured data and points to the feasibility of addressing the case, considering the deformed volume compatibility between the embankment and the underlying subsoil.

3.2 Existing analytical models

Moreover, another three analytical models (Hewlett and Randolph, 1988; Nordic Guideline, 2003; EBGEO, 2010) for the three-dimensional situation are presented to calculate the stress on the column top and that on the subsoil. The tensile forces in the geosynthetic reinforcement for these existing methods are determined using the following equation:

$$T = \frac{\sigma_u s_n}{2b}\sqrt{1+\frac{1}{6\varepsilon}} \tag{29}$$

where ε is the tensile strain and b is the width of the column in a square pattern. Eq. (29) is used for the case without the support of subsoil (BS8006, 2010; Van Eekelen et al., 2011; Chen et al., 2016b). In the proposed model, the modulus ratio of E_c/E_s = 100 is defined as the ultimate state, in which case no support comes from subsoil. This assumption was also made in Deb et al.'s study (2013). At the ultimate state, first, the vertical stress supported by the geosynthetic reinforcement is calculated. Eq. (29) can then be used to calculate the tensile force in the geosynthetics. Because this equation is used for a two-dimensional situation, for the axisymmetric model in this study, the column width and column spacing are obtained by transferring the axisymmetric model into a square pattern (Smith and Filz, 2007). ε = 2% is adopted to design the geosynthetics at the serviceability limit state to avoid localized differential settlement at the embankment surface.

The calculated results from these existing methods and the proposed model are tabulated in Tables 3 and 4. As mentioned, two scenarios–at the end of embankment construction and after paving the concrete base and rail plate–were considered. Compared with these existing methods, the stresses on the column top from the proposed model were close to that obtained from EBGEO (2010). An increase in the pressure on the geosynthetics is examined using the proposed model when applying a surcharge loading, that is, paving the concrete base and rail plate (Zhuang et al., 2016). However, the other three existing methods cannot present the tensile force change in the geosynthetics.

4. Parametric study

Based on the proposed method, a parametric study was performed. Various parameters, such as the embankment height, column spacing, column length, and so on, were examined. The properties related to the embankment system in different cases are presented in Table 5. Fig. 3 illustrates the variation of the stress ratio, σ_c/σ_s, with and without a geosynthetic reinforcement. The column spacing is set as d_e/d_c = 4. The results, with and without said reinforcement, are shown in this figure simultaneously. In the model with the reinforcement, the stresses above and below it are investigated. Compared to the results without a reinforcement, a relatively larger stress ratio was obtained below the geosynthetic reinforcement, whereas a relatively smaller ratio was calculated above this reinforcement. This is because some of the load supported by the subsoil transfers onto the column top via the reinforcement, resulting in the stress declining on the surrounding soil while increasing on the column under the geosynthetics. On the opposite side of the geosynthetic reinforcement, because the latter diminishes the deformation difference between the column and the subsoil, it supports some part of the load, consequently, yields a smaller stress ratio.

Fig. 4 further illustrates the impacts of column spacing and the modulus ratio on the change of σ_c/σ_s. When the column spacing grows in a certain range, the stress ratio increases accordingly. Meanwhile, a large modulus ratio can enhance the stress ratio counterpart, but the growth rate slows down after the modulus ratio reaches E_c/E_s = 50. Furthermore, the results with a geosynthetic reinforcement are presented in this figure. Compared to the solutions without the geosynthetic reinforcement, the stress ratios are enhanced to a certain degree, which means that said reinforcement can advance the load transfer efficiency. This conclusion is in accordance with the finding in Van Eekelen et al.'s study (2012a, 2012b).

Fig. 5 shows the variations in the stress at the column top and those in the foundation soil versus the modulus ratio, E_c/E_s. When widening the column spacing, the stress at the column top increases, whereas the stress on the foundation soil decreases within a small range. The increment percentage is defined as the stress increment because of the embedded geosynthetic reinforcement, compared to that without this reinforcement. The reader may observe that a larger increment percentage ((+) for the stress at the column top and (–) for the stress on the surrounding soil) appears with a relatively small modulus ratio. Thereafter, the increment percentage decreases, finally reaching a constant. This means that increasing the stiffness of the column cannot enhance the function of the geosynthetic reinforcement. The cost and load transfer efficiency should be balanced in real practice.

The effect of the embankment height on the load transfer is illustrated in Fig. 6. With the modulus ratio, E_c/E_s, growing, the stress ratio increases and finally approaches a constant. The embankment height appears to have little influence on the stress ratio without a geosynthetic reinforcement in dash lines. These curves almost overlap each other. However, when the geosynthetic reinforcement is applied, the results, in solid lines, separate from one another for different embankment heights. Moreover, the stress ratio is enlarged slightly with a relatively large embankment height. This means that the increasing rate in the stress at the column top is larger than that on the surrounding soil because of the embedded geosynthetic reinforcement.

Fig. 7 shows the change in the ratio of h_e/s_n with an increase in the embankment height, where s_n denotes the net column spacing. h_e, the height of the equal settlement plane, can represent the range of the load transfer platform or the height of soil arching. The observer may see that h_e decreases with a rise in the embankment height, meaning that with an increase in the uniform additional loading, the height of the equal settlement plane, h_e, is reduced. This is because the stress distribution below the equal settlement plane extends to a larger range. The load transfer occurs in a smaller range, resulting in a smaller h_e. Meanwhile, with an increase in the column spacing, the ratio of h_e/s_n decreases because the widening rate of the column spacing is larger than that of h_e. However, this ratio remains larger than 0.5, which is compatible with the dome height obtained by Hewlett and Randolph (1988).

Fig. 8 presents the variation of h_e versus the modulus ratio, E_c/E_s. In accordance with the behavior of the stress ratio, a large value in the modulus ratio can enlarge the value of h_e. However, the increasing rate slows down after the modulus ratio, E_c/E_s, becomes larger than 50. This means that the soil arching may be formed completely after the modulus ratio increases to a certain degree. The influence of the geosynthetic stiffness on h_e is also investigated, and the result without a geosynthetic reinforcement is introduced to make a comparison. The reader may note that the geosynthetic reinforcement can reduce the height of the equal settlement plane, h_e, while it can be shortened further by increasing its tensile stiffness. Fig. 9 describes the variation in the tensile force of the geosynthetic reinforcement with an increase in the modulus ratio. A large modulus ratio equates to a relatively larger deformation in the foundation soil than that in the column. The function of geosynthetic reinforcement is to diminish this differential settlement, which results in an increase in the tensile force. Moreover, extending the column spacing can lead to an increase of the tensile force in the geosynthetic reinforcement as well.

Fig. 10 shows the variation of the stress ratio, σ_c/σ_s, versus different column lengths with or without a geosynthetic reinforcement. With a relatively small column spacing, the stress ratio appears to remain constant with an increase in the depth of the foundation soil. However, with a growth in the column spacing, the stress ratio will first increase to a certain degree, before its acceleration rate slows down. This stress ratio then remain constant, even if increasing the depth of the column. This means that the settlement of the subsoil is in connection with the column spacing and mainly develops at the upper part of the foundation. Moreover, when the geosynthetic reinforcement is applied, the stress ratio increases accordingly, especially with a large column spacing.

Fig. 11 presents the variations in the stress ratio and in the value of h_e (i.e., equal settlement plane) with the increase of column length without a geosynthetic reinforcement. The influence of the embankment height is considered. The viewer can observe that increasing the embankment height cannot enhance the load transfer efficiency; that is, the stress ratio remains constant when increasing the embankment height. However, the height of the equal settlement plane decreases gradually. These features are consistent with the solutions of Figs. 7 and 8, meaning that, when increasing the embankment height, the range of the load transfer zone decreases. Because the increasing height of the embankment fill results in a large vertical stress in the load transfer platform, it increases the shear resistance at the potential slip surface. The load transfer evolves in a small range of the load transfer platform (height of equal settlement plane).

Fig. 12 illustrates the variation in h_e versus the column length with a geosynthetic reinforcement. The reader may discern that with a small value in the modulus ratio, E_c/E_s (Fig. 12a), or in the column spacing ratio, d_e/d_c (Fig. 12b), the column length (i.e., the thickness of subsoil) has little effect on the value of h_e. However, with a relatively large value in E_c/E_s (Fig. 12a), or in d_e/d_c (Fig. 12b), h_e increases when the column length is extended and remains constant after the column reaches a certain depth, meaning that a relatively significant depth of foundation soil has little influence on the height of the load transfer platform (i.e., equal settlement plane). This is in accordance with the result in Fig. 10.

Fig. 13 shows the change in the stress ratio during the construction process of the embankment fill. The viewer may find that, without the geosynthetic reinforcement, the stress ratio remains constant after the embankment height has reached a certain level (Fig. 13a). This means that the soil arching is completely formed, and increasing the embankment height has no effect on the stress ratio. However, with the embedded geosynthetic reinforcement (Fig. 13b), the stress ratio becomes larger compared to that without such a reinforcement. Furthermore, after reaching the equal settlement plane, the stress ratio keeps growing slightly with the embankment height. This illustrates that the geosynthetic reinforcement has a sustaining impact on the load transfer with an increase in the uniform additional loading.

Fig. 14 displays the variation of the maximum settlement in the surrounding soil with an increase in the embankment height. When the column spacing is enlarged, the settlement increases. However, an inflection point exists with a large column spacing, which appears around the equal settlement plane. This means that, before the soil arching forms, the settlement expands continuously with the increase in the embankment height. However, when the height reaches a certain level, which is close to that of the corresponding equal settlement plane, the load arches onto the adjacent column and the stress on the surrounding soil decreases, which results in a relatively small settlement. When the height is beyond the equal settlement plane, the stress on the surrounding soil continues to increase, as does the settlement accordingly.

Fig. 15 describes the tensile force of geosynthetic reinforcement versus the embankment height. The observer may note that, with an increase in said height, the value of the tensile force goes up, but decreases around the equal settlement plane. However, when the height exceeds the equal settlement plane, the tensile force continues to increase because of the increasing uniform additional loading (or self-weight of embankment). This is fairly similar to the trend of maximum settlement in subsoil (Fig. 14). Figs. 16 and 17 show the variations of maximum settlement and tensile force under different modulus ratios, E_c/E_s. Compared to Figs. 14 and 15, similar trends are observed in these figures. The difference is that the modulus ratio in Figs. 16 and 17 has a slight influence on the position of the inflection point, while the column spacing in Figs 14 and 15 has an obvious effect on the same.

5. Conclusions

In the present research, an axisymmetric model was performed for a geosynthetic-reinforced and column-supported embankment. A cylindrical unit cell was idealized from this type of embankment system, which combines the embankment fill with a geosynthetic reinforcement and the column-reinforced foundation soil. The load transfer mechanism and the equal settlement plane were investigated, bearing in mind the deformed volume continuity in the unit cell. The finding was that the geosynthetic reinforcement can increase the load transfer efficiency to a certain degree while reducing the height of the equal settlement plane. The application of a uniform additional loading (or increasing the height of the embankment) can condense the soil arching, resulting in a relatively low height of the equal settlement plane, but it is always larger than half of the column net spacing. In contrast, a large modulus disparity between the column and the subsoil results in an equal settlement plane of relatively significant height.

Acknowledgement

The authors would like to acknowledge the funding support from the Macau Science and Technology Development Fund (FDCT) (Code: 125/2014/A3), the National Natural Science Foundation of China (Grant no. 51508585, 51678319) and the University of Macau Research Fund (MYRG2017-00198-FST, MYRG2015-00112-FST). This project has received funding from the Marie Skłodowska-Curie Actions Research and Innovation Staff Exchange programme under grant agreement No [778360].

References

Abu-Farsakh, M., Hanandeh, S., Mohammad, L., Chen, Q., 2016. Performance of geosynthetic reinforced/stabilized paved roads built over soft soil under cyclic plate loads. Geotext. Geomembr. 44, 845–853.

Abusharar, S.W., Zheng, J.J., Chen, B.G., Yin, J.H., 2009. A simplified method for analysis of a piled embankment reinforced with geosynthetics. Geotext. Geomembr. 27, 39–52.

Alamgir, M., Miura, N., Poorooshasb, H.B., Madhav, M.R., 1996. Deformation analysis of soft ground reinforced by columnar inclusions. Comput. Geotech. 18, 267–290.

Ali, K., Shahu, J.T., Sharma, K.G., 2012. Model tests on geosynthetic-reinforced stone columns: a comparative study. Geosynth. Int. 19, 292–305.

Ariyarathne, P., Liyanapathirana, D.S., Leo, C.J., 2013. Effect of geosynthetic creep on reinforced pile-supported embankment systems. Geosynth. Int. 20, 421–435.

Ariyarathne, P., Liyanapathirana, D.S., 2015. Review of existing design methods for geosynthetic-reinforced pile-supported embankments. Soils Found. 55, 17–34.

Balaam, N.P., Booker, J.R., 1981. Analysis of rigid rafts supported by granular piles. Int. J. Numer. Anal. Methods Geomech. 5, 379–403.

Basack, S., Buddhima, I., Rujikiatkamjorn, C., 2015. Modeling the performance of stone column – reinforced soft ground under static and cyclic loads. J. Geotech. Geoenviron. Eng. 142, 1–15. https://doi.org/10.1061/(ASCE)GT.1943-5606.0001378.

Bhasi, A., Rajagopal, K., 2015. Numerical study of basal reinforced embankments supported on floating/end bearing piles considering pile–soil interaction. Geotext. Geomembr. 43, 524–536.

Bian, X., Jiang, H., Chen, Y., 2016. Preliminary testing on high-speed railway substructure due to water level changes. Procedia Eng. 143, 769–781.

Bordoloi, S., Yamsani, S.K., Garg, A., Sreedeep, S., Borah, S., 2015. Study on the efficacy of harmful weed species Eicchornia crassipes for soil reinforcement. Ecol. Eng. 85, 218–222.

Bordoloi, S., Kashyap, V., Garg, A., Sreedeep, S., Wei, L., Andriyas, S., 2018. Measurement of mechanical characteristics of fiber from a novel invasive weed: A comprehensive comparison with fibers from agricultural crops. Meas. J. Int. Meas. Confed. 113, 62–70.

Briançon, L., Simon, B., 2012. Performance of Pile-Supported Embankment over Soft Soil: Full-Scale Experiment. J. Geotech. Geoenviron. Eng. 138, 551–561.

Briançon, L., Simon, B., 2017. Pile-supported embankment over soft soil for a high-speed line. Geosynth. Int. 1–13.

BS8006, 2010. Code of practice for strengthened/reinforced soils and other fills. British Standard Institution, United Kingdom.

Cao, W.Z., Zheng, J.J., Zhang, J., Zhang, R.J., 2016. Field test of a geogrid-reinforced and floating pile-supported embankment. Geosynth. Int. 23, 348–361.

Chen, Y., Cao, W., Chen, R., 2008a. An experimental investigation of soil arching within basal reinforced and unreinforced piled embankments. Geotext. Geomembr. 26, 164–174.

Chen, R.P., Chen, Y.M., Han, J., Xu, Z.Z., 2008b. A theoretical solution for pile-supported embankments on soft soils under one-dimensional compression. Can. Geotech. J. 45, 611–623.

Chen, R.P., Jiang, P., Ye, X.W., Bian, X.C., 2016a. Probabilistic analytical model for settlement risk assessment of high-speed railway subgrade. J. Perform. Constr. Facil. 30, 4015047-1–10.

Chen, R.P., Xu, Z.Z., Chen, Y.M., Ling, D.S., Zhu, B., 2010. Field tests on pile-supported embankments over soft ground. J. Geotech. Geoenviron. Eng. 136, 777–785.

Chen, R.P., Wang, Y.W., Ye, X.W., Bian, X.C., Dong, X.P., 2016b. Tensile force of geogrids embedded in pile-supported reinforced embankment: A full-scale experimental study. Geotext. Geomembr. 44, 157–169.

Da Silva, E.M., Justo, J.L., Durand, P., Justo, E., Vázquez-Boza, M., 2017. The effect of geotextile reinforcement and prefabricated vertical drains on the stability and settlement of embankments. Geotext. Geomembr. 45, 447–461.

Das, A.K., Deb, K., 2017a. Modeling of stone column-supported embankment under axi-symmetric condition. Geotech. Geol. Eng. 35, 707–730.

Das, A.K., Deb, K., 2017b. Response of cylindrical storage tank foundation resting on tensionless stone column-improved soil. Int. J. Geomech. 17, 4016035.

Deb, K., 2010. A mathematical model to study the soil arching effect in stone column-supported embankment resting on soft foundation soil. Appl. Math. Model. 34, 3871–3883.

Deb, K., Mohapatra, S.R., 2013. Analysis of stone column-supported geosynthetic-reinforced embankments. Appl. Math. Model. 37, 2943–2960.

Debnath, P., Dey, A.K., 2017. Bearing capacity of reinforced and unreinforced sand beds over stone columns in soft clay. Geosynth. Int. 24, 575–589.

Disfani, M.M., Tsang, H., Arulrajah, A., Yaghoubi, E., 2017. Shear and Compression Characteristics of Recycled Glass-Tire Mixtures. J. Mater. Civ. Eng. 29(6), 6017003.

EBGEO, 2010. Emfehlungen für den entwurf und die berechnung von erdkorpern mit bewehrungen aus geokunststoffen. EBGEO, 2. German Geotechnical Society, Auflage.

Esmaeili, M., Zakeri, J.A., Babaei, M., 2017. Laboratory and field investigation of the effect of geogrid-reinforced ballast on railway track lateral resistance. Geotext. Geomembr. 45, 23–33. https://doi.org/10.1016/j.geotexmem.2016.11.003

Fagundes, D.F., Almeida, M.S.S., Thorel, L., Blanc, M., 2017. Load transfer mechanism and deformation of reinforced piled embankments. Geotext. Geomembr. 45, 1–10.

Feng, S.J., Ai, S.G., Chen, H.X., 2017a. Estimation of arching effect in geosynthetic-reinforced structures. Comput. Geotech. 87, 188–197.

Feng, S.J., Ai, S.G., Chen, H.X., Xie, H.J., 2017b. An analytical method for predicting load acting on geosynthetic overlying voids. Geotext. Geomembr. 45, 570–579.

Feng, S.J., Lu, S.F., 2015. Deformation analysis of a geosynthetic material subjected to two adjacent voids. Geotext. Geomembr. 43, 317–331.

Ghazavi, M., Ehsani Yamchi, A., Nazari Afshar, J., 2018. Bearing capacity of horizontally layered geosynthetic reinforced stone columns. Geotext. Geomembr. 46, 312–318. https://doi.org/10.1016/j.geotexmem.2018.01.002

Ghosh, B., Fatahi, B., Khabbaz, H., 2017a. Analytical solution to analyze LTP on column-improved soft soil considering soil nonlinearity. Int. J. Geomech. 17, 4016082.

Ghosh, B., Fatahi, B., Khabbaz, H., Yin, J.H., 2017b. Analytical study for double-layer geosynthetic reinforced load transfer platform on column improved soft soil. Geotext. Geomembr. 45, 508–536.

Girout, R., Blanc, M., Thorel, L., Dias, D., 2018. Geosynthetic reinforcement of pile-supported embankments. Geosynth. Int. 25, 37–49.

Girout, R., Blanc, M., Thorel, L., Fagundes, D.F., Almeida, M.S.S., Asce, M., 2016. Arching and deformation in a piled embankment: Centrifuge Tests Compared to Analytical Calculations. J. Geotech. Geoenviron. Eng. 142, 1–10.

Halvordson, K.A., Plaut, R.H., Filz, G.M., 2010. Analysis of geosynthetic reinforcement in pile-supported embankments. Part II: 3D plate model. Geosynth. Int. 17, 59–67.

Han, J., Gabr, M., 2002. Numerical analysis of geosynthetic-reinforced and pile-supported earth platforms over soft soil. J. Geotech. Geoenviron. Eng. 128, 44–53.

Hewlett, W.J., Randolph, M.F., 1988. Analysis of piled embankments. Gr. Eng. 21, 12–18.

Hinchberger, S.D., Rowe, R.K., 2003. Geosynthetic reinforced embankments on soft clay foundations: predicting reinforcement strains at failure. Geotext. Geomembr. 21, 151–175.

Hokmabadi, A.S., Fatahi, B., Samali, B., 2014. Assessment of soil-pile-structure interaction influencing seismic response of mid-rise buildings sitting on floating pile foundations. Comput. Geotech. 55, 172–186.

Hong, W.P., Lee, J., Hong, S., 2014. Full-Scale Tests on Embankments Founded on Piled Beams. J. Geotech. Geoenviron. Eng. 140, 04014067.

Huang, J., Han, J., 2009. 3D coupled mechanical and hydraulic modeling of a geosynthetic-reinforced deep mixed column-supported embankment. Geotext. Geomembr. 27, 272–280.

Huckert, A., Briançon, L., Villard, P., Garcin, P., 2016. Load transfer mechanisms in geotextile-reinforced embankments overlying voids: Experimental and analytical approaches. Geotext. Geomembr. 44, 442–456.

Iglesia, G.R., Einstein, H.H., Whitman, R. V., 2014. Investigation of Soil Arching with Centrifuge Tests. J. Geotech. Geoenviron. Eng. 140, 04013005.

Indraratna, B., Sun, Q., Heitor, A., Grant, J., 2018. Performance of rubber tire-confined capping layer under cyclic loading for railroad conditions. J. Mater. Civ. Eng. 30(3), 06017021.

Jamsawang, P., Yoobanpot, N., Thanasisathit, N., Voottipruex, P., Jongpradist, P., 2016. Three-dimensional numerical analysis of a DCM column-supported highway embankment. Comput. Geotech. 72, 42–56.

Jelušič, P., Žlender, B., 2018. Optimal design of piled embankments with basal reinforcement. Geosynth. Int. In press. https://doi.org/10.1680/jgein.17.00039

Jiang, Y., Han, J., Zheng, G., 2014. Numerical analysis of a pile-slab-supported railway embankment. Acta Geotech. 9, 499–511.

Jing, X.Y., Zhou, W.H., Zhu, H.X., Yin, Z.Y., Li, Y., 2018. Analysis of soil-structural interface behavior using three-dimensional DEM simulations. Int. J. Numer. Anal. Methods Geomech. 42, 339–357.

Jones, B.M., Filz, G.M., Plaut, R.H., 2010. Analysis of geosynthetic reinforcement in pile-supported embankments. Part I: 3D plate model. Geosynth. Int. 17, 59–67.

Kamash, W. El, Han, J., 2014. Displacements of column-supported embankments over soft clay after widening considering soil consolidation and column layout: Numerical analysis. Soils Found. 54, 1054–1069.

Karim, M.R., Manivannan, G., Gnanendran, C.T., Lo, S.-C.R., 2011. Predicting the long-term performance of a geogrid-reinforced embankment on soft soil using two-dimensional finite element analysis. Can. Geotech. J. 48, 741–753.

King, D.J., Bouazza, A., Gniel, J.R., Rowe, R.K., Bui, H.H., 2018. Geosynthetic reinforced column supported embankments and the role of ground improvement installation effects. Can. Geotech. J. 55, 792–809.

King, D.J., Bouazza, A., Gniel, J.R., Rowe, R.K., Bui, H.H., 2017. Serviceability design for geosynthetic reinforced column supported embankments. Geotext. Geomembr. 1–19.

Lai, H.J., Zheng, J.J., Zhang, J., Zhang, R.J., Cui, L., 2014. DEM analysis of “soil”-arching within geogrid-reinforced and unreinforced pile-supported embankments. Comput. Geotech. 61, 13–23.

Li, A.L., Rowe, R.K., 2008. Effects of viscous behavior of geosynthetic reinforcement and foundation soils on the performance of reinforced embankments. Geotext. Geomembr. 26, 317–334.

Liu, H.L., Ng, C.W.W., Fei, K., 2007. Performance of a geogrid-reinforced and pile-supported highway embankment over soft clay: Case study. J. Geotech. Geoenviron. Eng. 133, 1483–1493.

Liu, H., Kong, G., Chu, J., Ding, X., 2015. Grouted gravel column-supported highway embankment over soft clay: case study. Can. Geotech. J. 52, 1725–1733.

Liu, K.W., Rowe, R.K., 2016. Performance of reinforced, DMM column-supported embankment considering reinforcement viscosity and subsoil's decreasing hydraulic conductivity. Comput. Geotech. 71, 147–158.

Liu, K.W., Rowe, R.K., Su, Q., Liu, B., Yang, Z., 2017. Long-term reinforcement strains for column supported embankments with viscous reinforcement by FEM. Geotext. Geomembr. 45, 307–319.

Liu, S., Du, Y., Yi, Y., Puppala, A.J., 2012. Field investigations on performance of T-shaped deep mixed soil cement column supported embankments over soft ground. J. Geotech. Geoenviron. Eng. 138, 718–727.

Liyanapathirana, D.S., Ekanayake, S.D., 2016. Application of EPS geofoam in attenuating ground vibrations during vibratory pile driving. Geotext. Geomembr. 44, 59–69.

Low, B., Tang, S., Choa, V., 1994. Arching in Piled Embankments. J. Geotech. Eng. 120, 1917–1938.

Meguid, M.A., Hussein, M.G., Ahmed, M.R., Omeman, Z., Whalen, J., 2017. Investigation of soil-geosynthetic-structure interaction associated with induced trench installation. Geotext. Geomembr. 45, 320–330.

Mehdizadeh, A., Disfani, M.M., Evans, R., Arulrajah, A., 2018. Progressive Internal Erosion in a Gap-Graded Internally Unstable Soil: Mechanical and Geometrical Effects. Int. J. Geomech. 18, 4017160.

Michalowski, R.L., Wojtasik, A., Duda, A., Florkiewicz, A., Park, D., 2018. Failure and remedy of column-supported embankment: Case study. J. Geotech. Geoenviron. Eng. 144, 05017008.

Naggar, H. El, Turan, A., Valsangkar, A., 2015. Earth pressure reduction system using geogrid- reinforced platform bridging for buried utilities. J. Geotech. Geoenviron. Eng. 141, 04015024.

Nguyen, Q.V., Fatahi, B., Hokmabadi, A.S., 2017. Influence of size and load-bearing mechanism of piles on seismic performance of buildings considering soil-pile-structure interaction. Int. J. Geomech. 4017007, 1–22.

Nordic Geosynthetic Group, 2003. Nordic guidelines for reinforced soils and fills. Nordic Geotechnical Society, Stockholm, Stockholm.

Okyay, U.S., Dias, D., Thorel, L., Rault, G., 2014. Centrifuge modeling of a pile-supported granular earth-platform. J. Geotech. Geoenviron. Eng. 140, 04013015.

Pham, M.T., Briançon, L., Dias, D., Abdelouhab, A., 2018. Investigation of load transfer mechanisms in granular platforms reinforced by geosynthetics above cavities. Geotext. Geomembr. 46, 611–624.

Plaut, R.H., Filz, G.M., 2010. Analysis of geosynthetic reinforcement in pile-supported embankments part III: Axisymmetrical mdoel. Geosynth. Int. 17, 77–85.

Premkumar, S., Piratheepan, J., Arulrajah, A., Disfani, M.M., Rajeev, P., 2016. Experimental Study on Contact Erosion Failure in Pavement Embankment with Dispersive Clay. J. Mater. Civ. Eng. 28, 4015179.

Rowe, R.K., Liu, K., 2015. Three-dimensional finite element modelling of a full-scale geosynthetic-reinforced, pile-supported embankment. Can. Geotech. J. 52, 2041–2054.

Rowe, R.K., Li, A.L., 2005. Geosynthetic-reinforced embankments over soft foundations. Geosynth. Int. 12, 50–85.

Rui, R., Van Tol, F., Xia, X.L., Van Eekelen, S., Hu, G., Xia, Y.Y., 2016. Evolution of soil arching; 2D DEM simulations. Comput. Geotech. 73, 199–209.

Sexton, B.G., McCabe, B.A., Karstunen, M., Sivasithamparam, N., 2016. Stone column settlement performance in structured anisotropic clays: the influence of creep. J. Rock Mech. Geotech. Eng. 8, 672–688.

Shukla, S.K., Chandra, S., 1994. A generalized mechanical model for geosynthetic-reinforced foundation soil. Geotext. Geomembr. 13, 813–825.

Smith, M., Filz, G., 2007. Axisymmetric numerical modeling of a unit cell in geosyn thetic-reinforced, column-supported embankments. Geosynth. Int. 14, 13–22.

Smith, C.C., Tatari, A., 2016. Limit analysis of reinforced embankments on soft soil. Geotext. Geomembr. 44, 504–514.

Su, L.J., Yin, J.H., Zhou, W.H., 2010. Influences of overburden pressure and soil dilation on soil nail pull-out resistance. Comput. Geotech. 37, 555–564.

Suleiman, M.T., Ni, L., Davis, C., Lin, H., Xiao, S., 2016. Installation effects of controlled modulus column ground improvement piles on surrounding soil. J. Geotech. Geoenviron. Eng. 142, 04015059.

Taha, A., El Naggar, M.H., Turan, A., 2014. Experimental and numerical study on lateral behaviour of geosynthetic-reinforced pile foundation system. Geosynth. Int. 21, 352–363.

Tai, P., Indraratna, B., Rujikiatkamjorn, C., 2018. Experimental simulation and mathematical modelling of clogging in stone column. Can. Geotech. J. 55, 427–436.

Tan, S., Tjahyono, S., Oo, K., 2008. Simplified plane-strain modeling of stone-column reinforced ground. J. Geotech. Geoenviron. Eng. 134, 185–194.

Tano, B.F.G., Stoltz, G., Coulibaly, S.S., Bruhier, J., Dias, D., Olivier, F., Touze-Foltz, N., 2018. Large-scale tests to assess the efficiency of a geosynthetic reinforcement over a cavity. Geosynth. Int. 25, 242–258.

Terzaghi, K., 1943. Theoretical soil mechanics. John Wiley & Sons, New York.

Van Eekelen, S.J.M., 2016. The 2016-update of the Dutch design guideline for basal reinforced piled embankments. Procedia Eng. 143, 582–589.

Van Eekelen, S.J.M., Bezuijen, A., Lodder, H.J., Van Tol, A.F., 2012a. Model experiments on piled embankments. Part I. Geotext. Geomembr. 32, 69–81.

Van Eekelen, S.J.M., Bezuijen, A., Lodder, H.J., Van Tol, A.F., 2012b. Model experiments on piled embankments. Part II. Geotext. Geomembr. 32, 82–94.

Van Eekelen, S.J.M., Bezuijen, A., van Tol, A.F., 2015. Validation of analytical models for the design of basal reinforced piled embankments. Geotext. Geomembr. 43, 56–81.

Van Eekelen, S.J.M., Bezuijen, A., Van Tol, a. F., 2013. An analytical model for arching in piled embankments. Geotext. Geomembr. 39, 78–102.

Van Eekelen, S.J.M., Bezuijen, A., van Tol, a. F., 2011. Analysis and modification of the British Standard BS8006 for the design of piled embankments. Geotext. Geomembr. 29, 345–359.

Van Eekelen, S.J.M., Venmans, A.A.M., Bezuijen, A., van Tol, A.F., 2017. Long term measurements in the Woerden geosynthetic-reinforced pile-supported embankment. Geosynth. Int. 1–15.

Wang, H.L., Chen, R.P., Cheng, W., Qi, S., Cui, Y.J., 2018a. Full-scale model study on variations of soil stress in geosynthetic-reinforced pile-supported track-bed with water level change and loading cycles. Can. Geotech. J. In press.

Wang, H. L., Chen, R. P., Liu, Q. W., Kang, X., and Wang, Y.W., 2018b. Investigation on soil-geogrid interaction at various influencing factors by pullout tests with applications of FBG sensors. J. Mater. Civ. Eng. In press. https://doi.org/10.1061/(ASCE)MT.1943-5533.0002537

Wang, H.L., Chen, R.P., Qi, S., Cheng, W., Cui, Y.J., 2018c. Long-term performance of pile-supported ballastless track-bed at various water levels. J. Geotech. Geoenviron. Eng. 144, 04018035. https://doi.org/10.1061/(ASCE)GT.1943-5606.0001890

Villard, P., Huckert, A., Briançon, L., 2016. Load transfer mechanisms in geotextile-reinforced embankments overlying voids: Numerical approach and design. Geotext. Geomembr. 44, 381–395.

Weng, X., Zhu, H., Chen, J., Liang, D., Shi, B., Zhang, C., 2014. Experimental investigation of pavement behavior after embankment widening using a fiber optic sensor network. Struct. Heal. Monit. 1–11. doi:10.1177/1475921714548935

Wijerathna, M., Liyanapathirana, D.S., 2018. Reliability-based performance of embankments improved with deep mixing considering spatial variability of material properties. ASCE-ASME J. Risk Uncertain. Eng. Syst. Part A Civ. Eng. 4, 04018035.

Xu, C., Song, S., Han, J., 2016. Scaled model tests on influence factors of full geosynthetic-reinforced pile-supported embankments. Geosynth. Int. 23, 140–153.

Yang, X., Han, J., 2013. Analytical model for resilient modulus and permanent deformation of geosynthetic-reinforced unbound granular material. J. Geotech. Geoenviron. Eng. 139, 1443–1453.

Yapage, N.N.S., Liyanapathirana, D.S., Poulos, H.G., Kelly, R.B., Leo, C.J., 2015. Numerical Modeling of Geotextile-Reinforced Embankments over Deep Cement Mixed Columns Incorporating Strain-Softening Behavior of Columns. Int. J. Geomech. 15, 4014047.

Yapage, N.N.S., Liyanapathirana, D.S., 2014. A parametric study of geosynthetic-reinforced column-supported embankments. Geosynth. Int. 21, 213–232.

Yin, J., Zhou, W., 2009. Influence of grouting pressure and overburden stress on the interface resistance of a soil nail. J. Geotech. Geoenviron. Eng. 135, 1198–1208.

Yin, Z.Y., Chang, C.S., Hicher, P.Y., 2010a. Micromechanical modelling for effect of inherent anisotropy on cyclic behaviour of sand. Int. J. Solids Struct. 47, 1933–1951.

Yin, Z.Y., Chang, C.S., Hicher, P.Y., Karstunen, M., 2009. Micromechanical analysis of kinematic hardening in natural clay. Int. J. Plast. 25, 1413–1435.

Yin, Z.Y., Chang, C.S., Karstunen, M., Hicher, P.Y., 2010b. An anisotropic elastic-viscoplastic model for soft clays. Int. J. Solids Struct. 47, 665–677.

Yin, Z.Y., Hattab, M., Hicher, P.Y., 2011a. Multiscale modeling of a sensitive marine clay. Int. J. Numer. Anal. Methods Geomech. 35, 1682–1702.

Yin, Z.Y., Hicher, P.-Y., Dano, C., Jin, Y.F., 2017. Modeling mechanical behavior of very coarse granular materials. J. Eng. Mech. 143, C4016006.

Yin, Z.Y., Karstunen, M., Chang, C.S., Koskinen, M., Lojander, M., 2011b. Modeling time-dependent behavior of soft sensitive clay. J. Geotech. Geoenviron. Eng. 137, 1103–1113.

Yoo, C., 2015. Settlement behavior of embankment on geosynthetic-encased stone column installed soft ground – A numerical investigation. Geotext. Geomembr. 43, 484–492.

Yu, Y., Bathurst, R.J., 2017. Influence of Selection of Soil and Interface Properties on Numerical Results of Two Soil – Geosynthetic Interaction Problems. Int. J. Geomech. ASCE 17, 1–16.

Yu, Y., Bathurst, R.J., Damians, I.P., 2016. Modified unit cell approach for modelling geosynthetic-reinforced column-supported embankments. Geotext. Geomembr. 44, 332–343.

Zhang, C., Jiang, G., Liu, X., Buzzi, O., 2016. Arching in geogrid-reinforced pile-supported embankments over silty clay of medium compressibility: Field data and analytical solution. Comput. Geotech. 77, 11–25.

Zhang, C.C., Zhu, H.H., Shi, B., Wu, F.D., Yin, J.H., 2015a. Experimental investigation of pullout behavior of fiber-reinforced polymer reinforcements in sand. J. Compos. Constr. 19, 4014062.

Zhang, C.C., Zhu, H.H., Xu, Q., Shi, B., Mei, G.X., 2015b. Time-dependent pullout behavior of glass fiber reinforced polymer (GFRP) soil nail in sand. Can. Geotech. J. 52, 671–681.

Zhao, L.S., Zhou, W.H., Fatahi, B., Li, X. Bin, Yuen, K.V., 2016. A dual beam model for geosynthetic-reinforced granular fill on an elastic foundation. Appl. Math. Model. 40, 9254–9268.

Zhao, L.S., Zhou, W.H., Yuen, K.V., 2017. A simplified axisymmetric model for column supported embankment systems. Comput. Geotech. 92, 96–107.

Zhou, W.H., Lao, J.Y., Huang, Y., Chen, R., 2017. Group effect on soil arching in geogrid-reinforced pile-supported embankments. Japanese Geotech. Soc. Spec. Publ. 5, 130–134.

Zhou, W.H., Yin, J.H., Hong, C.H., 2011. Finite element modelling of pullout testing on a soil nail in a pullout box under different overburden and grouting pressures. Can. Geotech. J. 48, 557–567.

Zhou, W., Chen, R., Zhao, L., Xu, Z., Chen, Y., 2012. A semi-analytical method for the analysis of pile-supported embankments. J. Zhejiang Univ. Sci. A 13, 888–894.

Zhou, W.H., Lao, J.Y., Huang, Y., Chen, R., 2016. Three-dimensional finite element modelling of soil arching in pile-supported geogrid-reinforced embankments. Procedia Eng. 143, 607–614.

Zhou, W.H., Yin, J.H., 2008. A simple mathematical model for soil nail and soil interaction analysis. Comput. Geotech. 35, 479–488.

Zhu, H., Zhou, W.H., Yin, Z.Y., 2017. Deformation mechanism of strain localization in 2D numerical interface tests. Acta Geotech. 13(3), 557–573.

Zhuang, Y., Wang, K.Y., 2015. Three-dimensional behavior of biaxial geogrid in a piled embankment: numerical investigation. Can. Geotech. J. 52, 1629–1635.

Zhuang, Y., Wang, K.Y., 2016. Finite-element analysis on the effect of subsoil in reinforced piled embankments and comparison with theoretical method predictions. Int. J. Geomech. 16, 4016011.

Zhuang, Y., Yu, K., Long, H., 2014. A simplified model to analyze the reinforced piled embankments. Geotext. Geomembr. 42, 154–165.

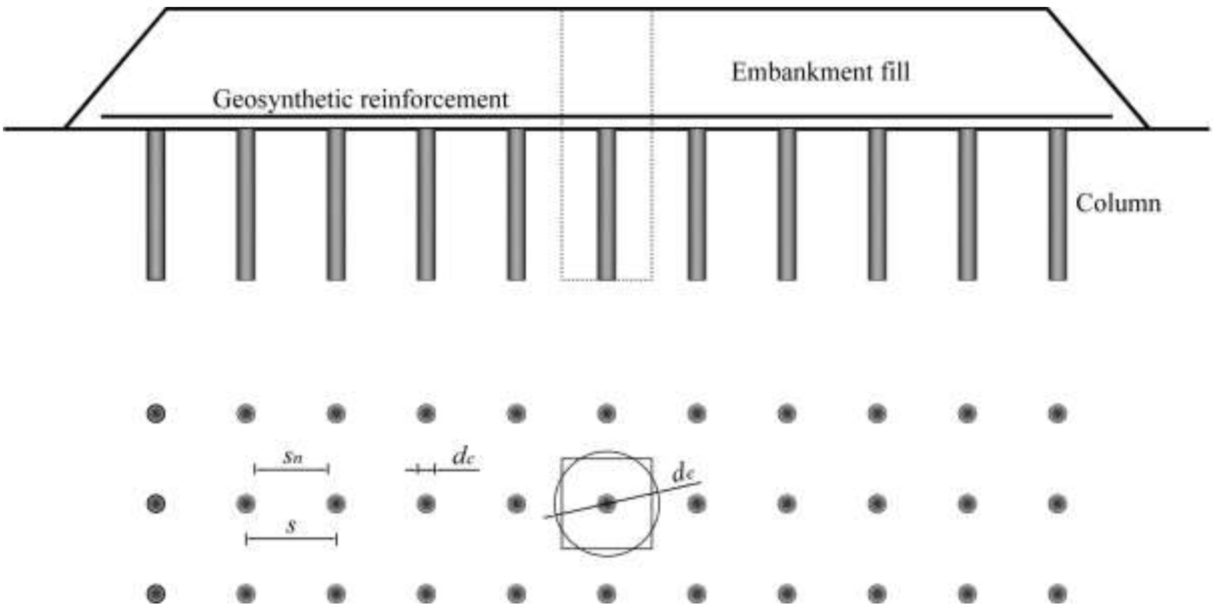

Fig. 1. Skech map of a geosynthetic-reinforced and column-supported embankment

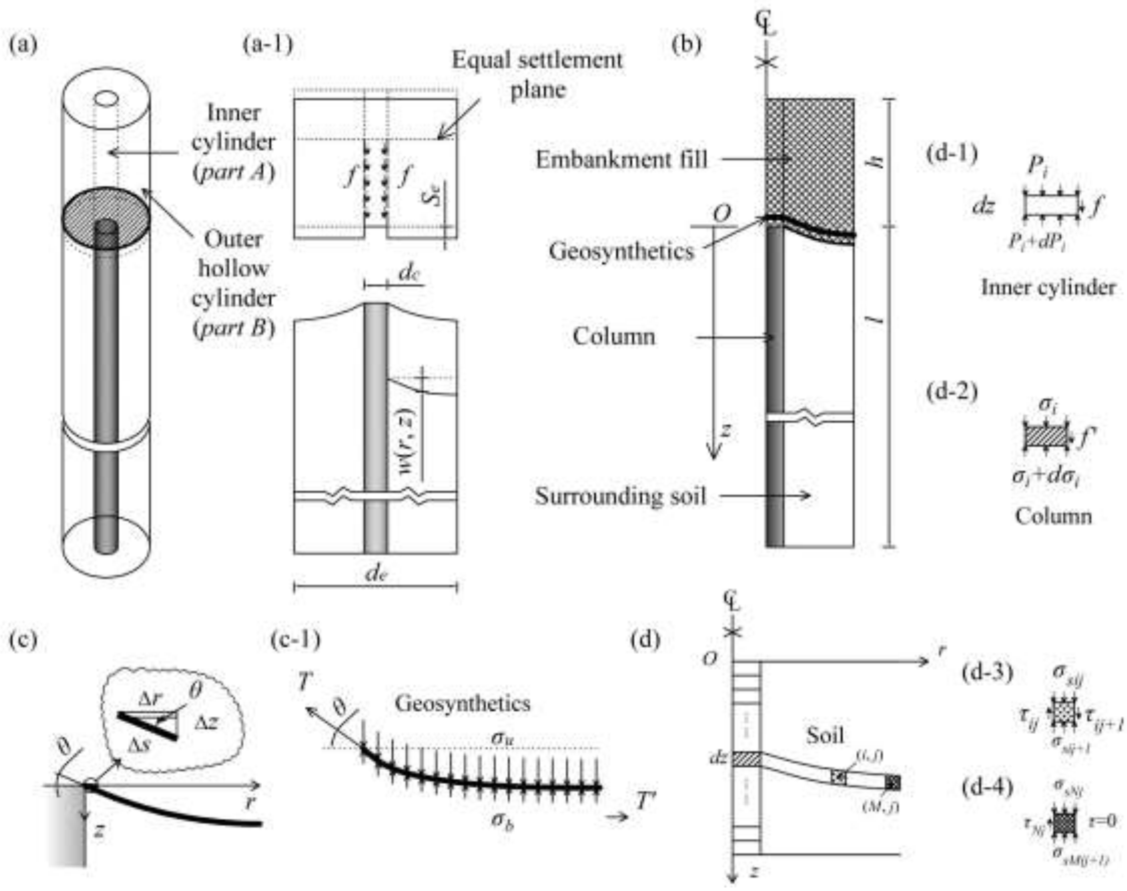

Fig. 2. (a) Cylindrical unit cell model; (b) Cross section of unit cell; (c) Deformation analysis diagram of geosynthetics; (d) Stresses in the inner cylinder, column and surrounding soil

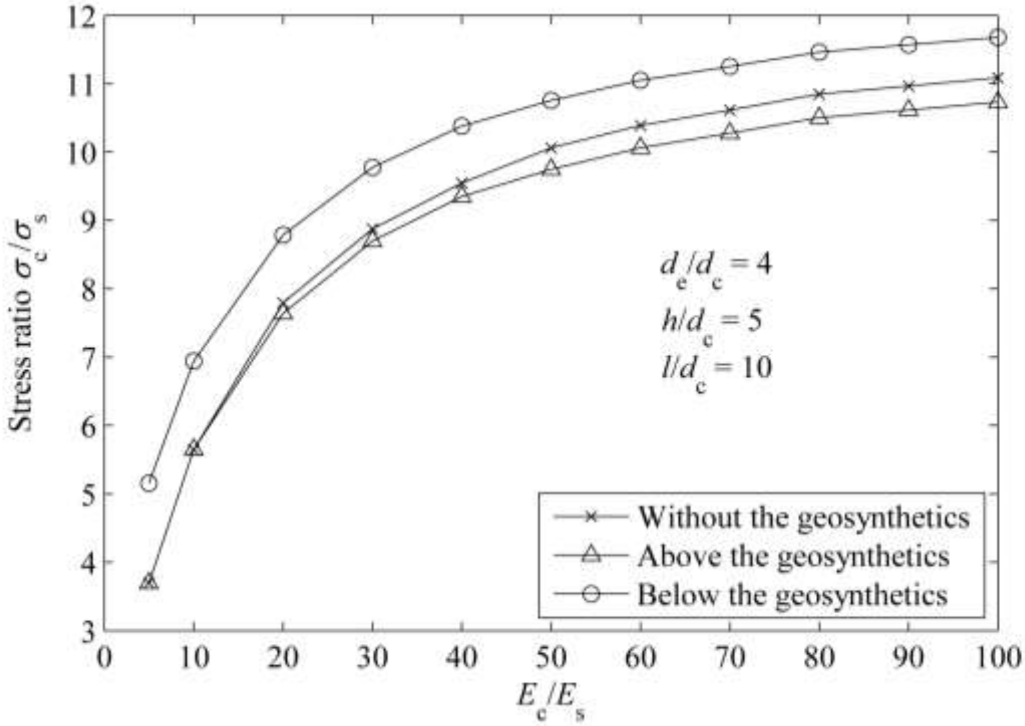

Fig. 3. Variation in the stress ratio versus modulus ratio, E_c/E_s, with and without a geosynthetic reinforcement

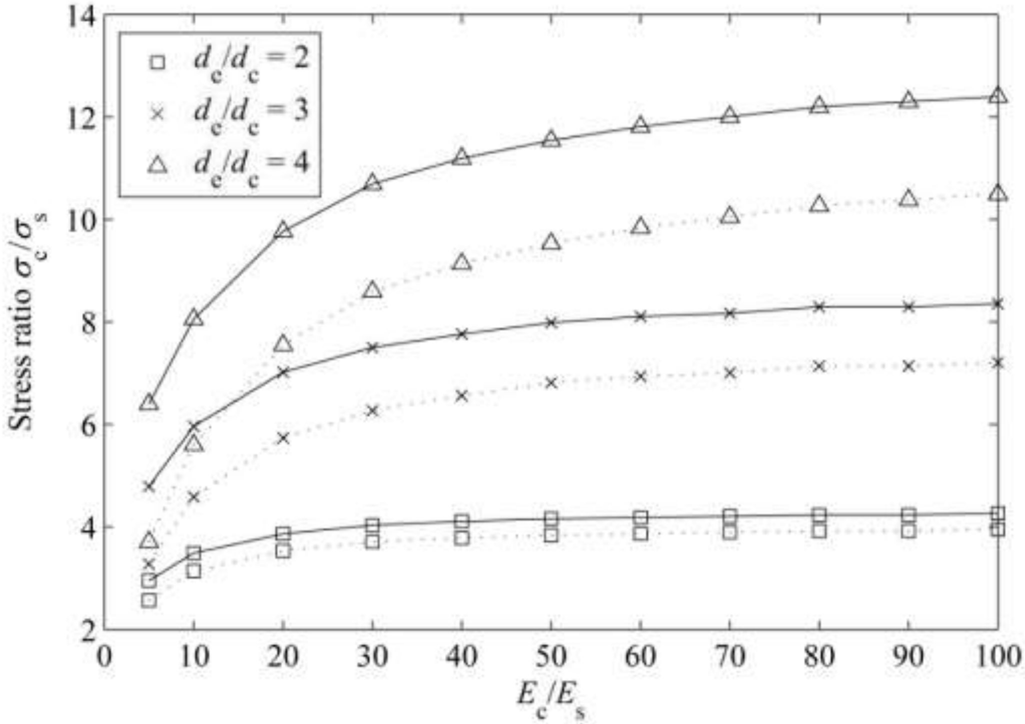

Fig. 4. Influence of geosynthetic reinforcement on the stress ratio versus modulus ratio, E_c/E_s

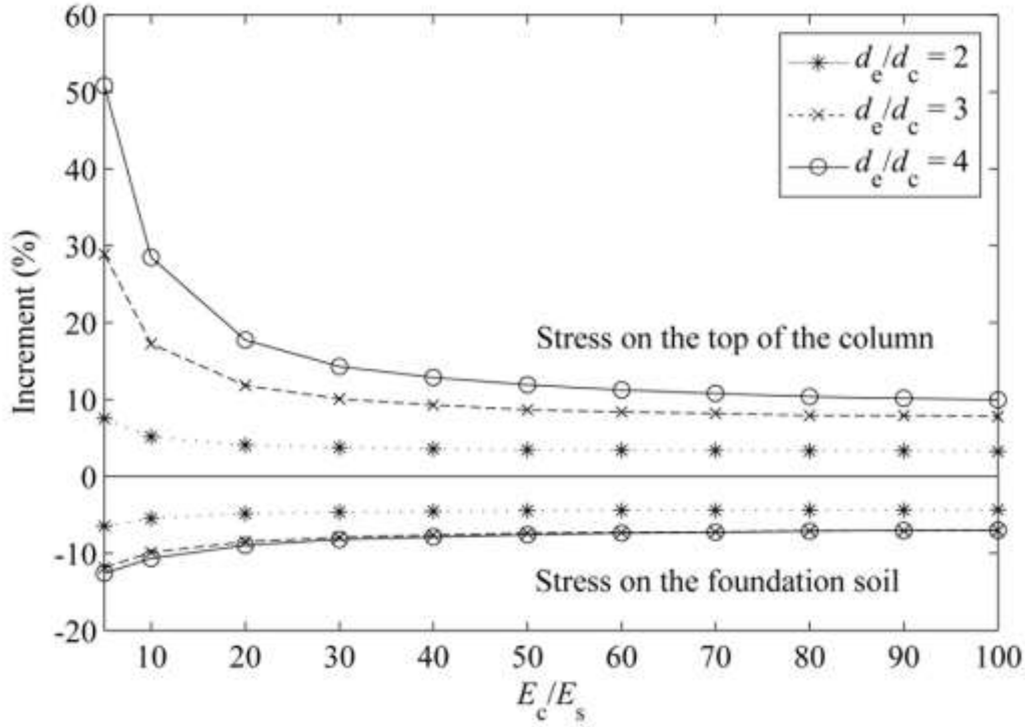

Fig. 5. Stress increment arising from the included geosynthetic reinforcement

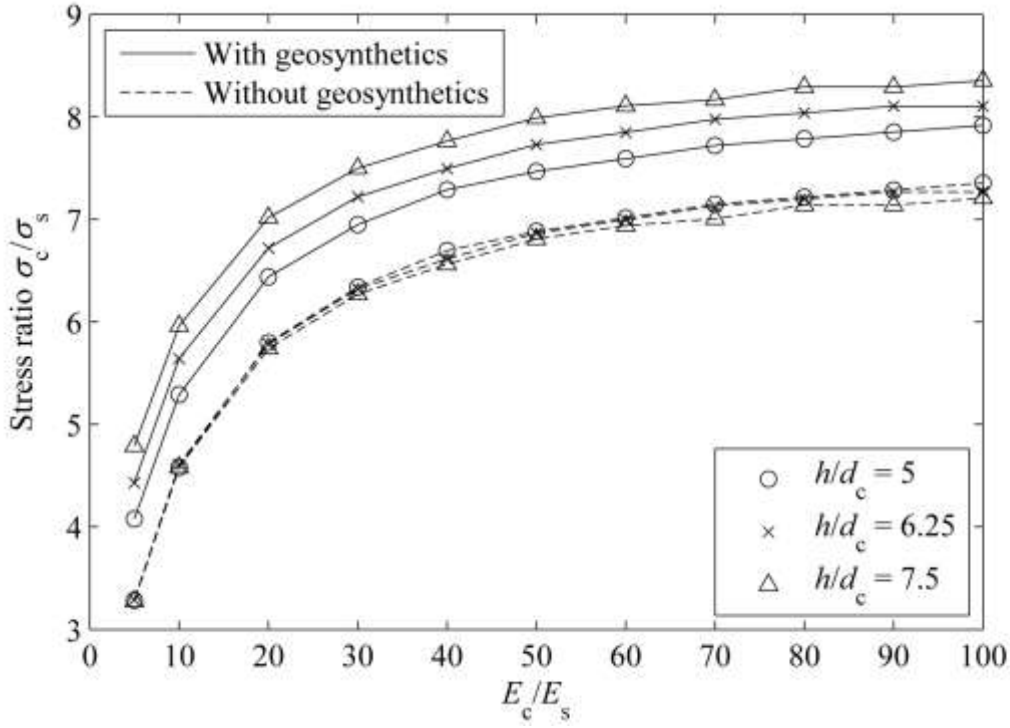

Fig. 6. Influence of embankment height on the stress ratio with and without the geosynthetic reinforcement

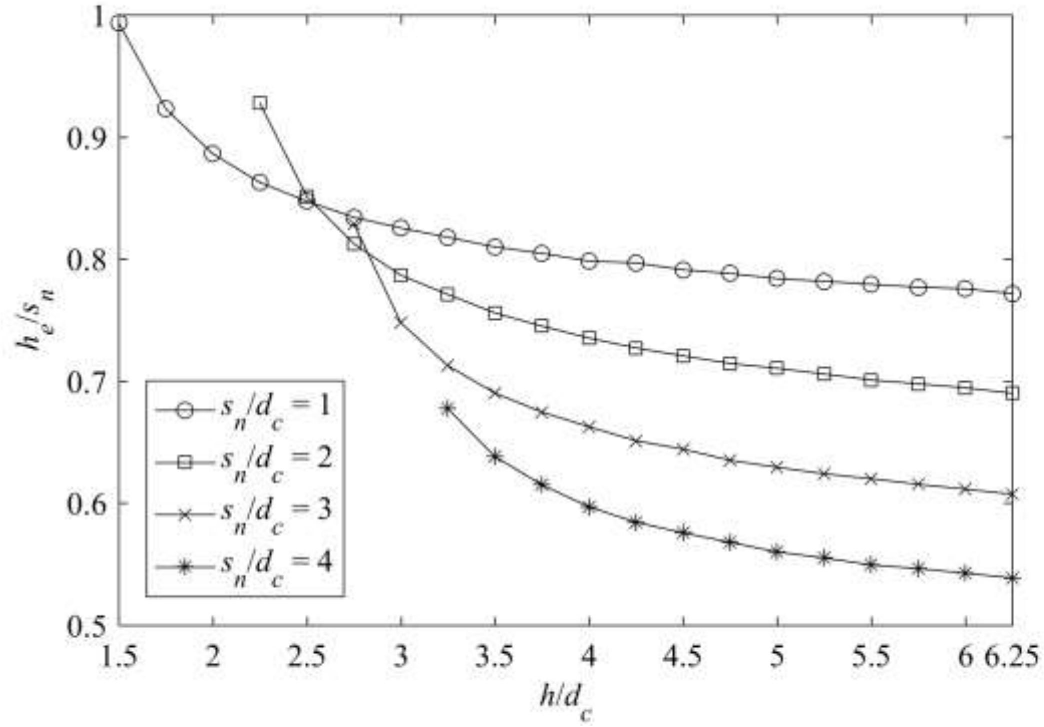

Fig. 7. Influence of embankment height on the ratio between h_e and s_n

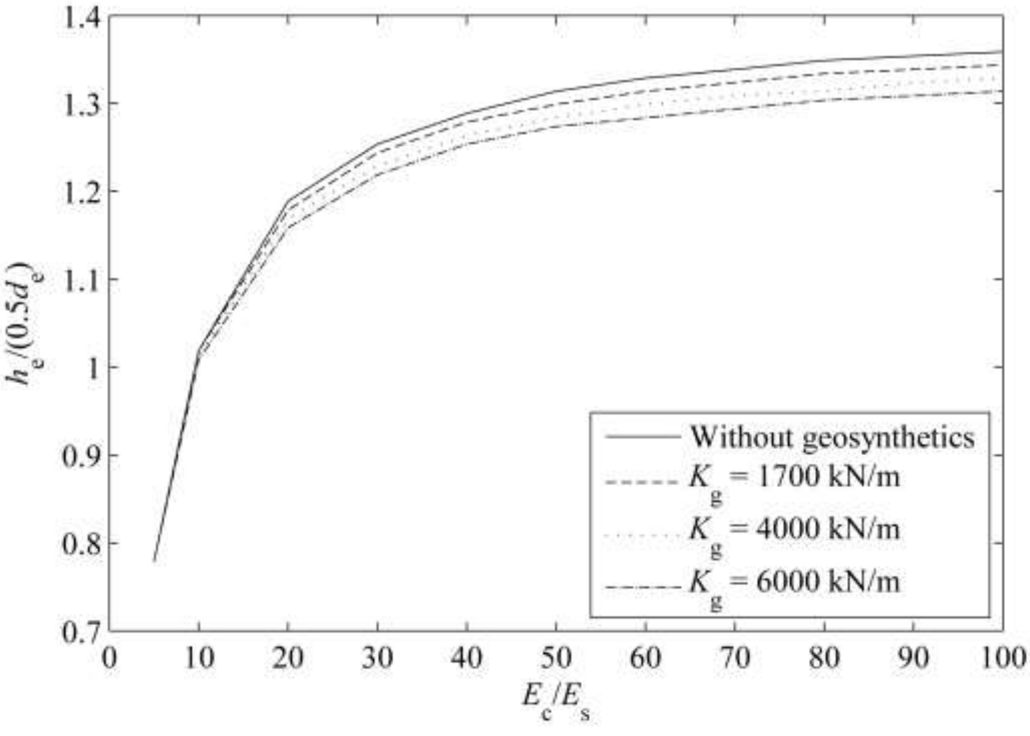

Fig. 8. Influence of geosynthetic stiffness on the height of equal settlement plane

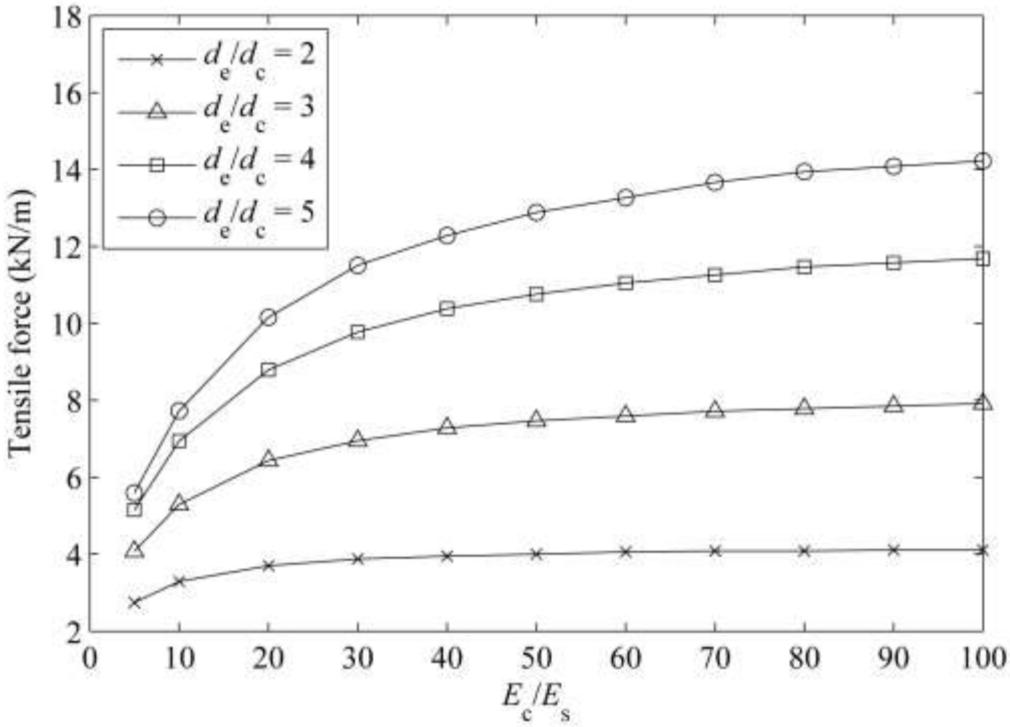

Fig. 9. Influence of column spacing on the tensile force versus modulus ratio

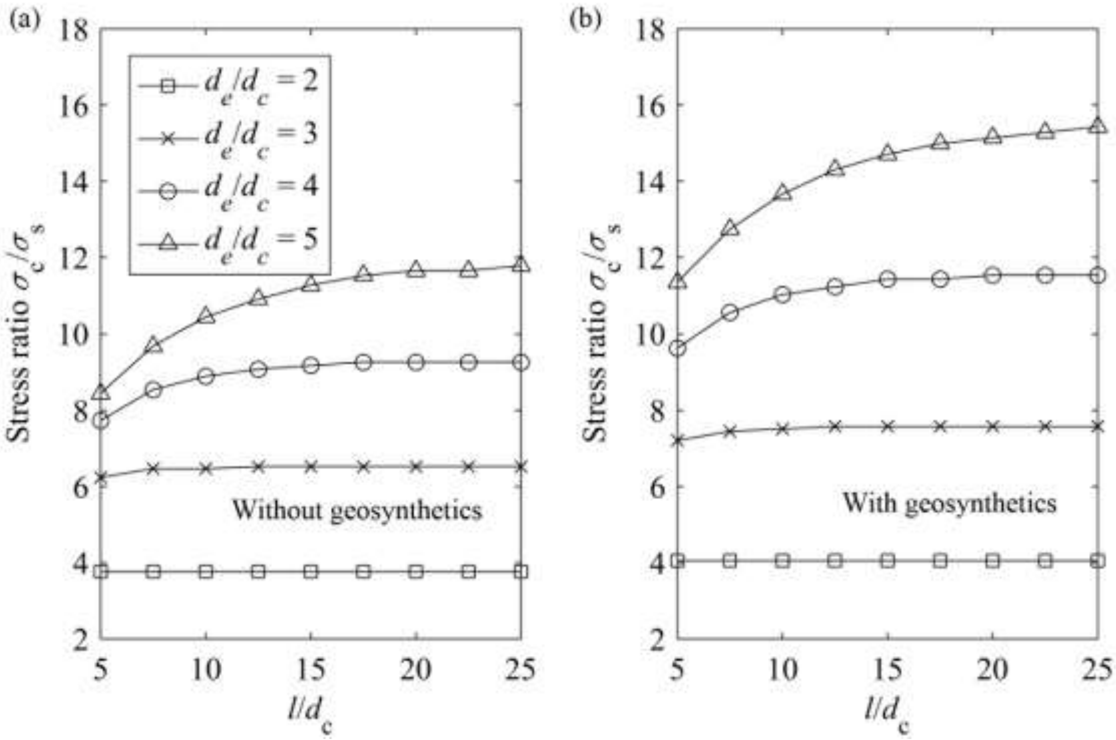

Fig. 10. Variation in the stress ratio with an increase in the length of column

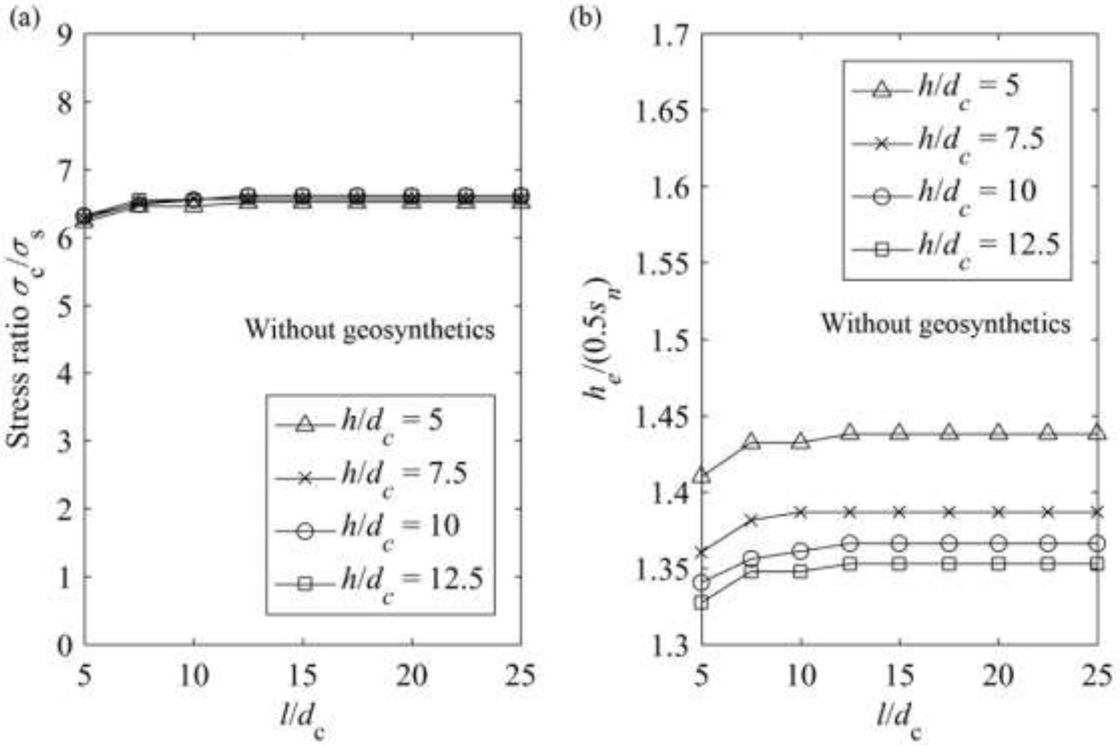

Fig. 11. Variation of stress ratio and height of equal settlement plane with different length of column

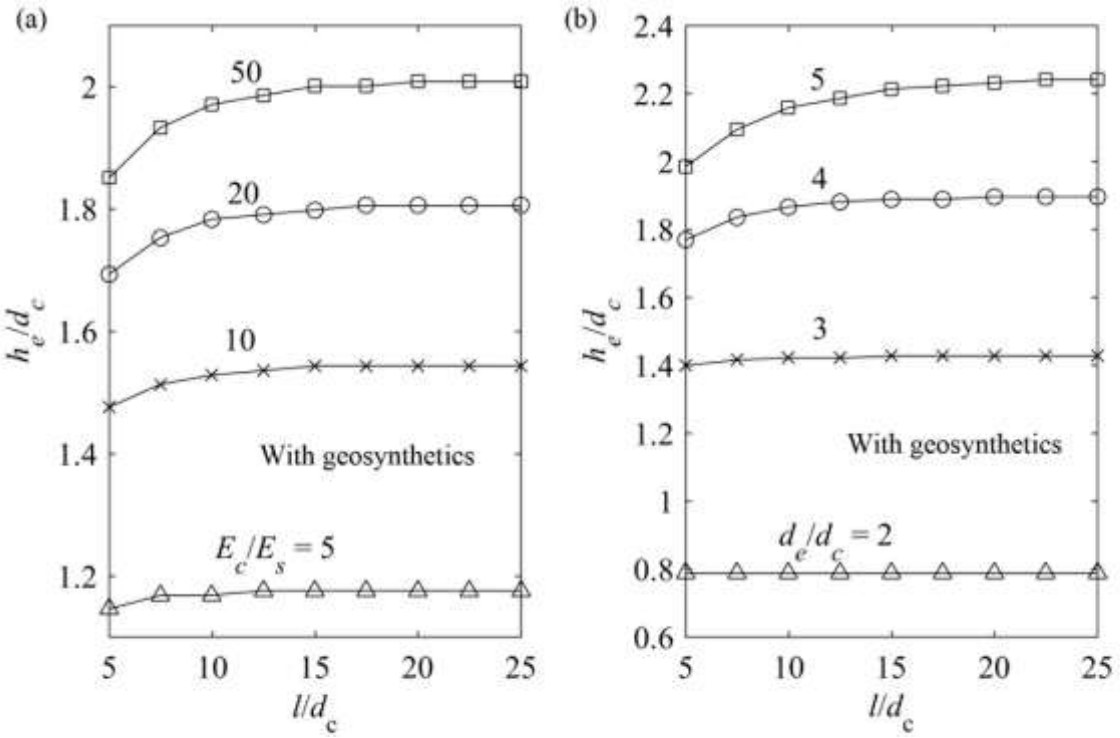

Fig. 12. Influence of (a) modulus ratio and (b) column spacing on the height of equal settlement plane

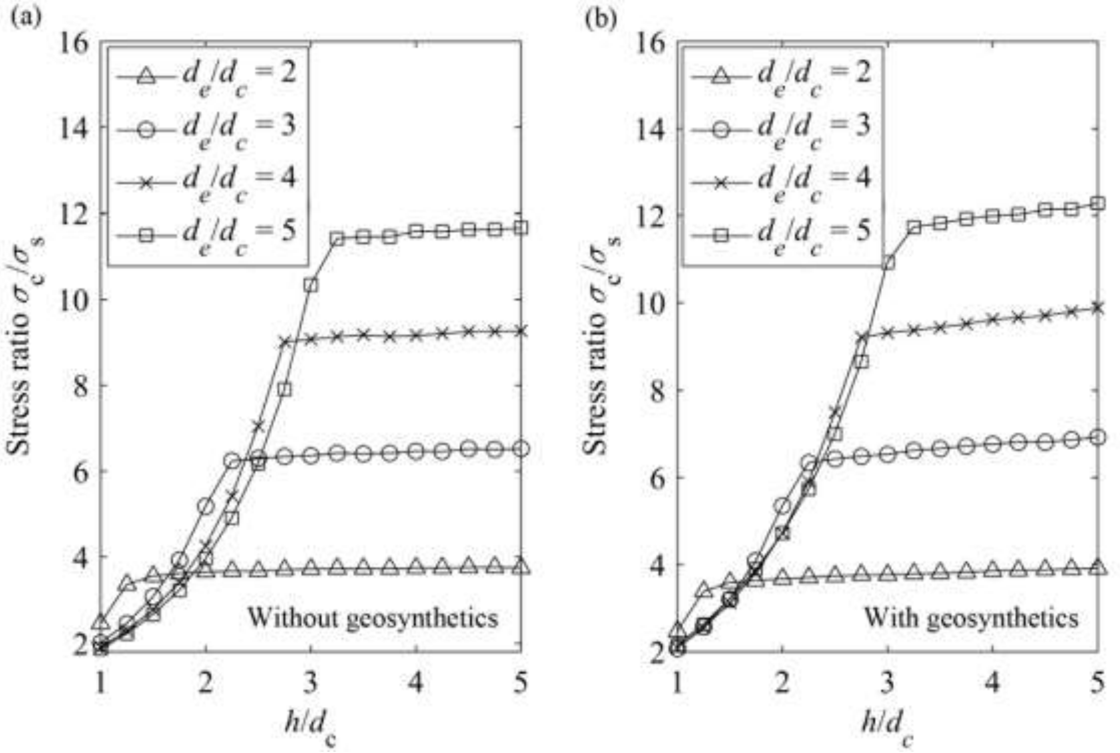

Fig. 13. Variation of stress ratio with an increase in the embankment height

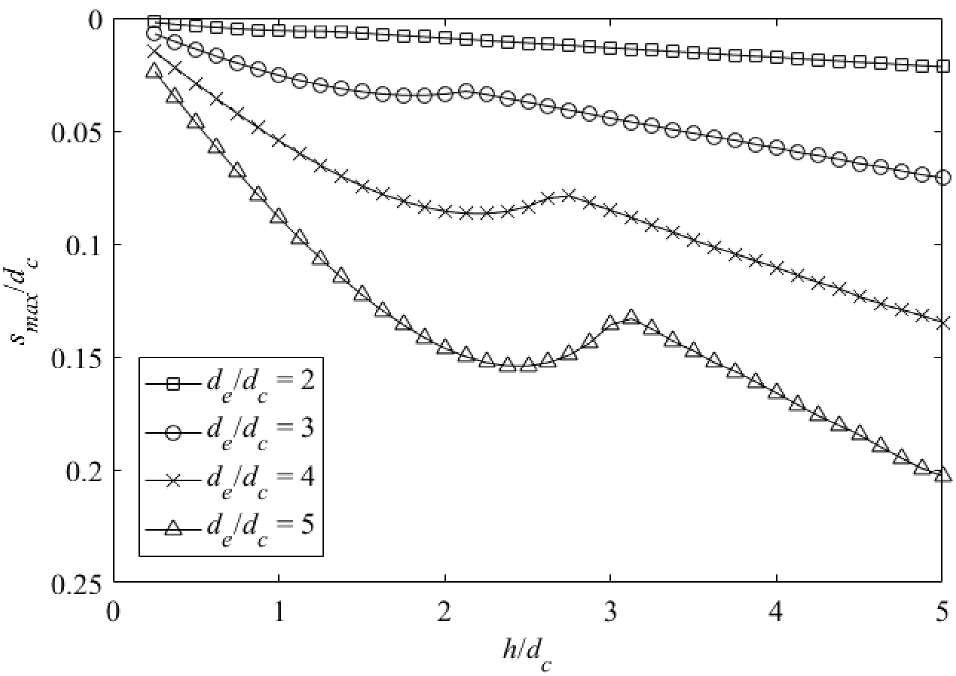

Fig. 14. Maximum settlement of foundation soil with an increase in the embankment height

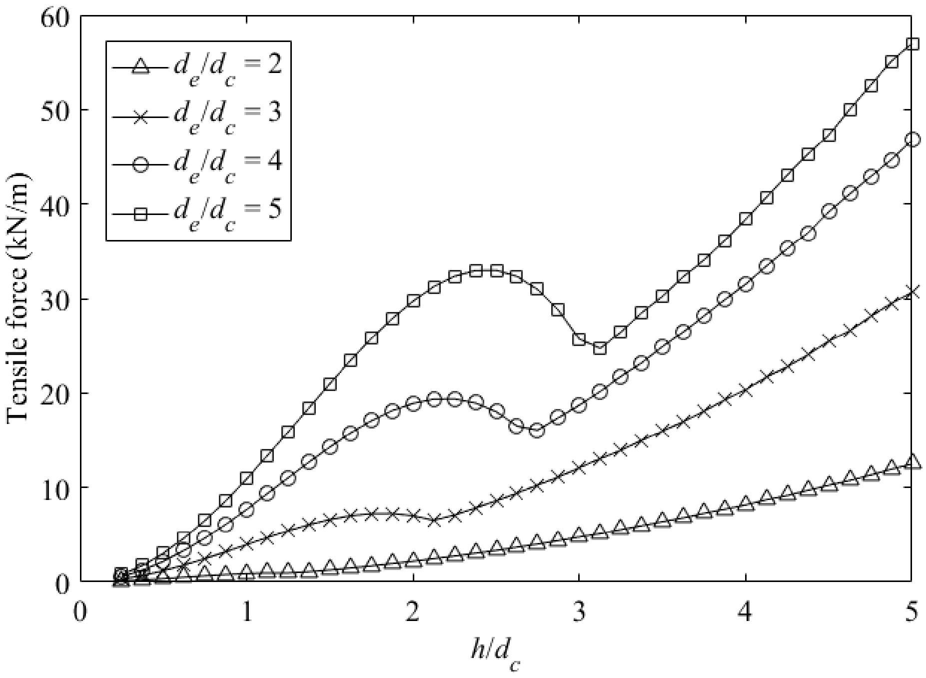

Fig. 15. Tensile force of geosynthetic reinforcement with an increase in the embankment height

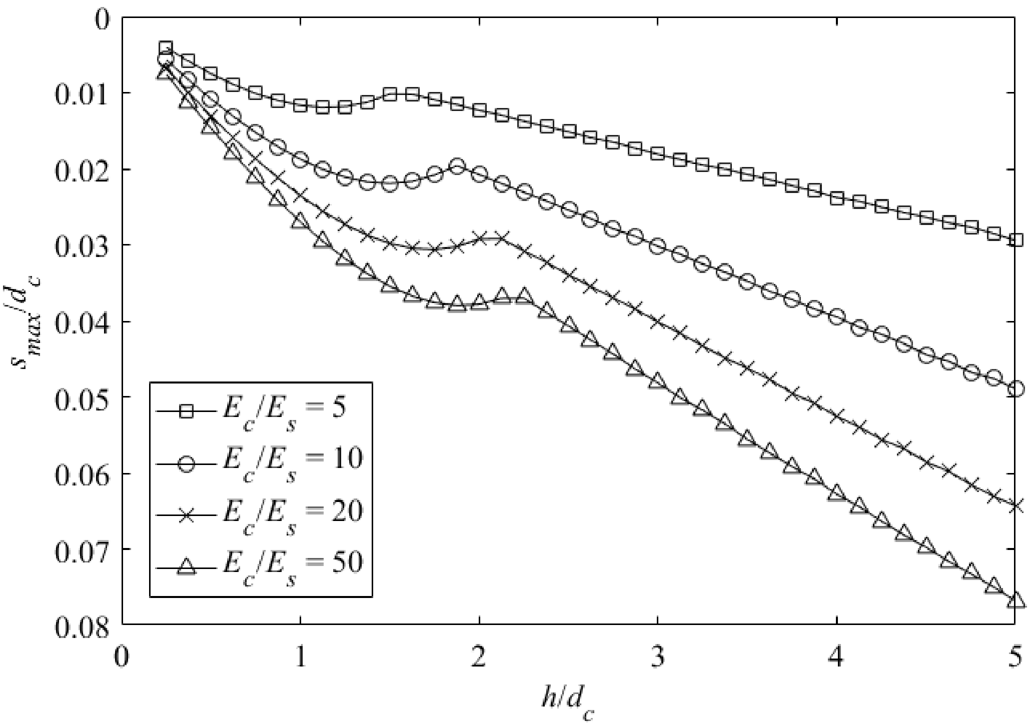

Fig. 16. Maximum settlement of foundation soil versus height of embankment fill

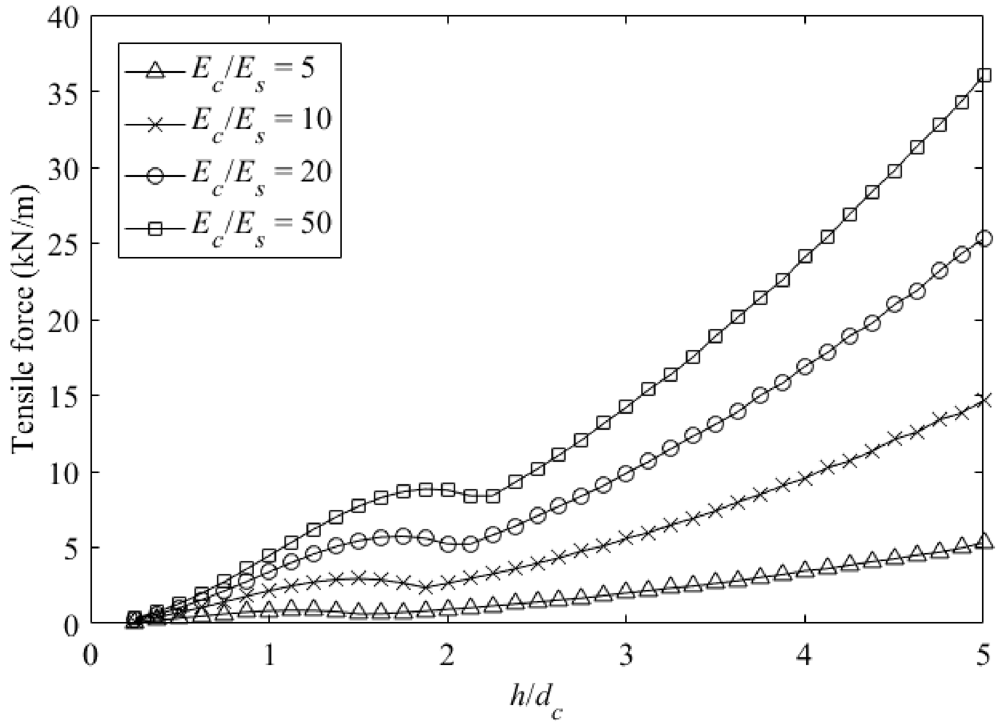

Fig. 17. Tensile force of geosynthetic reinforcement with an increase in embankment height

Table 1. Parameters for the design methods and proposed model

Parameters	Full-scale test	Proposed method
Fill height, h	3.2 m	3.2 m
Unit weight of the fill, γ	21.2 kN/m^3	21.2 kN/m^3
Modulus of the fill, E_f	(31.2–53.5) MPa	30 MPa
Friction angle, φ	43.6°	43.6°
Column spacing (circle), d_e	--	2.03 m
Column spacing (square)	1.8 m	--
Column diameter (circle), d_c	--	1.13 m
Column width (square)	1 m	--
Column length, l/d_c	--	20
Stiffness ratio, E_c/E_s	--	10
Poisson's ratio of soil, v_s	--	0.35
Concrete base and rail plate, q	12.25 kPa	12.25 kPa
Tensile stiffness of geosynthetics	2459.5 kN/m	2459.5 kN/m

Table 2. Comparison with a full-scale test (Chen et al., 2016b; Zhou et al., 2016)

		σ_c (kPa)	σ_s (kPa)	T (kN/m)
End of embankment construction	Measured data	158.4	27.4	3.8
	Proposed method	163.9	22.6	5.6
With concrete base and rail plate	Measured data	169.7	26.5	3.8
	Proposed method	186.6	24.8	6.2

Table 3. Comparison with design methods (End of embankment construction)

	σ_c (kPa)	σ_s (kPa)	T (kN/m)
Hewlett and Randolph (1988)	189	13.5	16.5
Nordic Guideline (2003)	180.9	17.3	21.1
EBGEO (2010)	205.1	6.6	8.1
Proposed model (ultimate state)	193	11.9	14.5

Table 4. Comparison with design methods (With concrete base and rail plate)

	σ_c (kPa)	σ_s (kPa)	T (kN/m)
Hewlett and Randolph (1988)	216.1	13.5	15.5
Nordic Guideline (2003)	207.6	17.3	21.1
EBGEO (2010)	231.2	6.8	8.3
Proposed model (ultimate state)	228.4	14	17.1

Table 5. Parameters used in the parametric study

	d_e/d_c	E_c/E_s	l/d_c	E_f/E_s	h/d_c	K_g (kN/m)
Fig. 3	4	--	25	3	5	1700
Fig. 4	--	--	25	3	5	1700
Fig. 5	--	--	25	3	5	1700
Fig. 6	3	--	25	3	--	1700
Fig. 7	--	30	25	3	5	--
Fig. 8	3	30	25	3	5	--
Fig. 9	--	--	25	3	--	1700
Fig. 10	--	30	--	3	--	1700
Fig. 11	3	30	--	3	--	1700
Fig. 12	--	--	--	3	5	1700
Fig. 13	--	30	25	3	5	1700
Fig. 14	--	30	20	3	--	1700
Fig. 15	--	30	20	3	--	1700
Fig. 16	3	--	20	3	--	1700
Fig. 17	3	--	20	3	--	1700